T.C.

ISTANBUL AYDIN UNIVERSITY

INSTITUTE OF GRADUATE

STUDIES

SYNTHETIC APERTURE RADAR SIGNAL PROCESSING

M.Sc. THESIS

ABUBAKAR YAOUBA

Department of Electrical and Electronics Engineering

Electrical and Electronics Engineering Program

April, 2020

T.C.

ISTANBUL AYDIN UNIVERSITY

INSTITUTE OF GRADUATE

STUDIES

SYNTHETIC APERTURE RADAR SIGNAL PROCESSING

M.Sc. THESIS

ABUBAKAR YAOUBA
(Y1713.300012)

Department of Electrical and Electronics Engineering

Electrical and Electronics Engineering Program

Thesis Advisor: Assist. Prof. Dr. NECİP GÖKHAN KASAPOĞLU

April, 2020

DECLARATION

I hereby declare that the information in this document which I submitted as a Master thesis, has been obtained and presented in accordance with academic rules and ethical conduct. I also declare that, as required by these rules and conduct, I have fully cited and referenced all material resulted that are not original to this work. The work has been done by myself under the supervision of my advisor and has not been submitted to any other institution for a diploma or a degree.

Abubakar Yaouba

FOREWARD

The completion of my Thesis work would not have been possible without all those who supported me in one way or the other.

First of all, I will like to express my sincere gratitude to my Thesis Advisor: **Assist. Prof. Dr. Necip Gökhan KASAPOĞLU**, who guided me to select a suitable topic for my thesis and also provided me with the necessary materials for this work. I thank him for everything I learned from him. He has been a source of inspiration and a guiding force behind this work.

I am very thankful to all, the lecturers of Istanbul Aydin University that supported me in one way or the other during the course of my studies. It was such a privilege to be opportune to receive lectures from them.

I am also obliged to **Assist. Prof. Dr. ANDREI ANGHEL** who gave the opportunity to work under him during the course of my studies at University Politehnica Bucharest Romania.

<u>April, 2020</u>   <u>**Abubakar Yaouba**</u>
(Electric and Electronic Engineer)

i

TABLE OF CONTENTS   **Pages**

LIST OF FIGURES

LIST OF TABLES

LIST OF ABBREVIATIONS

ADC   : Analog to Digital Converter

AM   : Amplitude Modulation

dB   : Decibels

DAC   : Differential Azimuth Compression

DFT   : Discrete Fourier Transform

DN   : Digital Number

ESA   : European Space Agency

FFT   : Fast Fourier Transform

FM   : Frequency Modulation

IFFT   : Inverse Fast Fourier Transform

IFP   : Image Focusing Plate

LFM   : Linear Frequency Modulation

LNA   : Low Noise Amplifier

LPF   : Low Pass Filter

NASA   : National Aeronautics and Space Administration

PA   : Power Amplifier

PAF   : Processing and Archiving Facility

PLFM   : Pulsed Linear Frequency Modulation

RCMC   : Range Cell Migration Correction

RDA   : Range Doppler Algorithm

SAR   : Synthetic Aperture Radar

SLAR   : Side Looking Airborne Radar

SLC   : Single Look Complex

SRC   : Secondary Range Compression

TOPS   : Terrain Observation by Progressive Scans

UAV   : Unmanned Aerial Vehicle

SYNTHETIC APERTURE RADAR SIGNAL PROCESSING

ABSTRACT

Synthetic aperture radar signal processing is a two-dimensional operation consisting of the range compression and the azimuth compression. SAR signal processing is very important for generating and processing of various data products for different applications and analysis of the target features. The SAR raw data are 2D array of sampled echoes in complex form. The practicality of the algorithms for SAR signal processing are used to compress the energy of the echoes, thereby increasing the resolution of the SAR image. In this work, it is shown how the Range-Doppler, Stolt Interpolation, and Chirp scaling techniques are carried out. The implementation of the differential azimuth compression (DAC) for the Stolt Interpolation algorithm, Secondary Range Compression (SRC) and Range Cell Migration Correction for Chirp scaling algorithm are presented and analyzed. The Range-Doppler, Stolt Interpolation, and Chirp scaling algorithms are demonstrated in Matlab and compared.

Keywords: *Range-Doppler algorithm, Stolt Interpolation, differential azimuth compression, Chirp scaling algorithm, Secondary Range Compression, Range Cell Migration Correction*

SENTETİK APERTÜR RADAR SİNYAL İŞLEME

ÖZET

Sentetik açıklıklı radar sinyal işleme, aralık sıkıştırması ve azimut sıkıştırmasından oluşan iki boyutlu bir işlemdir. Sentetik diyafram radar sinyal işleme, farklı uygulamalar için çeşitli veri ürünlerinin üretilmesi ve işlenmesi ve hedef özelliklerin analizi için çok önemlidir. Sentetik açıklıklı radar ham verileri, karmaşık formdaki örnek ekoların iki boyutlu dizisidir. Sentetik açıklık radarı sinyal işleme algoritmalarının pratikliği, yankıların enerjisini sıkıştırmak, böylece Sentetik açıklıklı radar görüntüsünün çözünürlüğünü arttırmak için kullanılır. Bu çalışmada Range-Doppler, Stolt Enterpolasyonu ve Chirp ölçekleme tekniklerinin nasıl gerçekleştirildiği gösterilmiştir. Stolt İnterpolasyon algoritması, Sekonder Aralık Sıkıştırma ve Chirp ölçekleme algoritması için Aralık Hücresi Göç Düzeltmesi için diferansiyel azimut sıkıştırma uygulaması sunulur ve analiz edilir. Range-Doppler, Stolt İnterpolasyon ve Chirp ölçekleme algoritmaları Matlab'da gösterilmiş ve karşılaştırılmıştır.

Anahtar Kelimeler: *Range-Doppler algoritması, Stolt İnterpolasyonu, diferansiyel azimut sıkıştırma, Chirp ölçekleme algoritması, İkincil Aralık Sıkıştırması, Aralık Hücresi Göç Düzeltmesi*

1.   INTRODUCTION

Synthetic Aperture Radar (SAR) is a type of technology where a radar sensor with a small real antenna is mounted on a moving platform such as airplanes, satellites, high altitude balloons, UAVs or drones to synthetically produce a high-resolution 2D or 3D images of objects such as landscapes. It generates and transmits a series of coded pulses at a regular interval as the platform moves along its path. The total distance the SAR device covers at a time when the backscattered signals are detected by the sensor creates a large virtual antenna known as a synthetic antenna aperture. That is, a large virtual antenna is synthesized using the displacement of the real antenna along the track. SAR operates in the microwave band, and it interacts with the target and then collects the corresponding echoes followed by imaging. Basically, microwave sensors are either passive sensors, that only detect natural radiation emitted from bodies such as the atmosphere or active sensors, that create microwave radiation to scan target objects [1]. Active sensors are categorized into imaging microwave sensors such as LIDAR and SAR as they can take a measurement in two dimensions and non-imaging microwave sensors such as scatterometer, altimeters, etc. that take measurements only in one dimension. SAR remote sensing technique that provides a fine spatial resolution of 2D data that does not depend on the height of the sensor. So images with the same geometric resolution can be obtained from the satellite as from airplanes. SAR's day-and-night imaging capability, weather independence, penetration of radar wave, geometric resolution, and independence of distance, makes the most popular imaging system for remote sensing technology [2].

Table 1. Comparing of SAR sensors and other remote sensing instruments

	Optical multi-spectral	Lidar	SAR
Platform	airborne/spaceborne/UAVs	Airborne/UAVs	Airborne/spaceborne/UAVs
Spectrum	Visible light/infrared	infrared	Microwave(radio)
Radiation	Reflected Sunlight	Own radiation	Own radiation
Frequency	Multi-frequency	Single frequency	Multi-frequency
Acquisition time	Day/night	Day	Day/night
Weather	Blocked by clouds	Blocked by clouds	See through clouds

The SAR transmits modulated signals and receives corresponding echoes at a fixed pulse repetition frequency towards a side looking direction. The pulse repetition frequency depends on the radar type and ranges from hundreds of KHz to thousands KHz for airborne and spaceborne systems. Table 2 below summarizes some of the commonly used frequency bands of SAR systems and their corresponding frequency ranges, and wavelengths [3], [4], [1]

Table 2. Frequency bands of SAR systems

Frequency Band	Frequency Range	Wavelength(cm)
mm	47GHz – 300GHz	0.75 – 0.1
Ka-Band	27GHz - 47GHz	0.75 - 1.2
K-Band	18GHz – 27GHZ	1.2 – 1.7
Ku-Band	14GHz - 18GHz	1.7 - 2.5
X-Band	8GHz - 12GHz	2.5 - 4
C Band	4GHz - 8GHz	4 - 8
S Band	2GHz - 4GHz	8 - 15
L Band	1GHz - 2GHz	15 - 30
P Band	300MHz - 1GHz	60 - 120

The Ka-band, K-band, and Ku-band are not usable for spaceborne radar remote sensing because of their small wavelengths that have high possibility to be blocked by the atmospheric particles or clouds. There is no currently available sensor for S-band and P-band [5], [1]

1.1. SAR History.

SAR systems were at first mounted on airborne platforms. Due to the rapid progress of radar technology and systems theory, leads to the development of spaceborne SAR systems. The first airborne SAR system was developed by Carl Wiley of the Goodyear Aerospace Corporation of the US in the 1950s [6]. In June 1978, the Seasat [7], was developed and launched by NASA, which carries the first spaceborne SAR in the world [8], [9]. Although it worked only for 105 days, it collected more information than that gathered by the marine ships over the past 100 years, proving the capability of spaceborne SAR system to collect information within a short period of time. Since this discovery in 1978, Spaceborne SAR system has gained the attention of scientific researchers in the world and spaceborne SAR sensors have greatly increased in number. Table 3 below shows some famous spaceborne SAR systems [8], [9].

In the nearest future, more spaceborne SAR sensors will be launched. ESA has programmed to launch a sensor in P-band in 2019/2020 named Biomass mission. With its long wavelength, it will be able to penetrate through the canopy cover. NISAR is to be launch in 2021. It will be a joint satellite mission between ISRO and NASA. It will be made up of two bands, the L-band provided by NASA and the S-band provided by ISRO. It will be applicable in the diction of inundation, change in water level in forested and Urban areas, flooding from runoff and snowmelt, extent and degree of mine collapse, etc. ISRO successfully launched RISAT-2B on May 22, 2019. A Spanish earth observation satellite PAZ was launched on February 22, 2018, from Vandenberg Air Force Base in California, United State. PAZ focuses on both space and Earth observation [5]. PAZ is positioned on the same German TerraSAR–X, and TanDEM–X radar satellites orbit.

Table 3. List of famous satellite systems

Satellite	Band Designated	Polarization	Agency	Year of Operation
ERS-1	C	VV	ESA	1991–2000
ERS-2	C	VV	ESA	1995–2011
JERS	L	HH	NASDA	1992–1998
RADARSAT-1	C	HH	CSA	1995–2013
RADARSA2	C (quad–pol)	polarimetric	CSA	2007
ENVISAT	C	polarimetric	ESA	2002–2012
ALOS 1	L (quad-pol)	polarimetric	JAXA	2006-2011
TerraSAT-X	X (quad-pol)	polarimetric	DLR	2007
COSMO-SkyMeD-1/4	X (dual)	polarimetric	DLR	2007
ALOS 2	L (quad-pol)	polarimetric	JAXA	2014
Tandem–X	X (quad-pol)	polarimetric	DLR	2010
RISAT-1	C	HH/HV	ISRO	2012
KOMPSAT–5	X(dual)	polarimetric	KARI	2013
Sentinel–1	C	HH/HV or VV/VH	ESA	2014

A constellation of more than two satellites will make images available faster in the future. The SAR also evolves from single polarization mode to multiple polarization modes, with bands ranging from X-band to P-band. Currently, SAR systems are being developed to achieve high resolution, high radiation resolution and accuracy, high temporal resolution and wide swath.

1.2. Different Type of SAR Systems:

SAR systems are categorized into Monostatic SAR system, Bistatic SAR system, and Multistatic SAR system.

1.2.1. Monostatic SAR Systems

Monostatic SAR systems uses single antenna to transmit and receive the reflected electromagnetic pulses. In this system, there is a ferrite multi-port circulator that directs the outgoing signal to the antenna and directs the returned signal to the receiver. Monostatic SAR is the principal configuration for most SAR systems operating today. The spaceborne SAR sensors are all monostatic SAR systems.

1.2.1.1.   Quasi-Monostatic Systems

The quasi-monostatic systems have both the transmitting and receiving antennas on the same radar slightly separated.

1.2.2. Bistatic SAR Systems

Bistatic SAR systems the transmitting antenna and receiving antenna are separately located (mounted) on two different platforms (spatially separated) for example, ground transmitter and satellite receiver [7]. The two Monostatic SAR systems TanDEM X and TerraSAR X with same configuration, flying closely with typical distances between 250m and 500m form a bistatic SAR system. In this case, one will act as a transmitter and the other as a receiver.

1.2.3. Multistatic SAR Systems

Multistatic SAR systems are divided into fully active Multistate radar system (Radars have both transmitting and receiving capability) and Semi-active Multistate radar system (One active transmitter with more passive receivers).

1.3.   Modes of SAR Operation.

Due to different SAR system configuration, SAR uses different methods to acquire data. Some of these methods are totally different systems such as Inverse SAR, Bistatic SAR and SAR interferometry and others are different modes of a system. The three basic modes include the spotlight mode, the Stripmap mode and the ScanSAR mode

1.3.1. Spotlight Mode

In this mode, the antenna beam is being steered continuously to focus on an area with narrow illumination spot to acquire longer synthetic aperture [3], [5], which can increase coherent integration time and gain better azimuth resolution. At a single pass, a high resolution image is generated at multiple viewing angles [10], [7]. This mode is a practical choice when collecting fine resolution data.

1.3.2. Stripmap Mode

In this mode, the look angle of the antenna is fixed relative to the flight line. The antenna beam sweeps an area parallel to the flight direction at constant rate obtaining a consecutive strip image. The antenna of the system is flexible to select different swaths by altering the incidence angle [3], [7]. Stripmap mode is a standard mode of SAR and the most commonly used. It could either be a broadside mode or a squint mode. In the broadside mode, the radar platform travels at constant velocity and altitude on a level flight direction and in squint mode, the antenna is either pointed forward or backward normal to the flight direction

a) Broadside Stripmap mode

c) Squint Stripmap mode
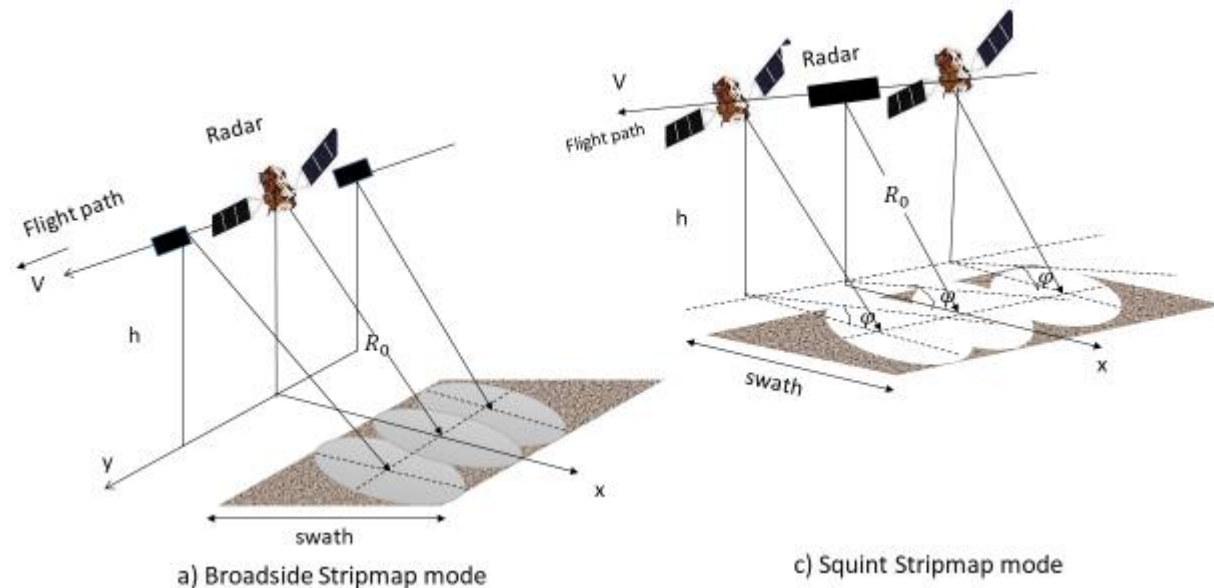
Figure 1.1. Stripmap mode

1.3.3. ScanSAR Mode

The ScanSAR mode or "Burst mode" is a wide-swath mode. It can be thought as the extension of Stripmap mode [7]. In ScanSAR, the sensor steers the antenna by changing the angle of elevation of the beam along the direction of flight to scan an area in range several times to achieve a wider swath coverage [3], [11], [5]. This allows imaging of a larger swath with degraded azimuth resolution. ScanSAR mode includes both the Stripmap and the spotlight modes as specific case.

1.3.4. Sliding Spotlight SAR Mode

Sliding Spotlight SAR evolved from Spotlight SAR. It can be thought of as the combination of Spotlight mode and Stripmap mode [11]. Its beam points at a certain virtual center which is far from the imaging all the time. The virtual center position far from the imaging can determine the velocity of the beam foot. Therefore, the coherent integration time can be increased and the azimuth resolution can be improved compared with Stripmap SAR. Sliding Spotlight SAR was actually proposed to increase the swath width in azimuth.

1.3.5. TOPS Mode

This mode is designed to remove the scalloping effects in ScanSAR. The antenna swings to illuminate the different sub-swaths and also images each target completely with the same whole antenna pattern by scanning the ground quickly from back to front in the azimuth direction. Unlike the sliding spotlight mode, the virtual rotating center is above the platform. Somehow it is equivalent to inverse sliding spotlight mode [3], [11]

1.3.6. Multi-channel Mode

In this mode high resolution in azimuth and wide swath in range can be achieved simultaneously. The antenna is made up of several sub-arrays which are distributed uniformly along the platform trajectory [11]. Each sub-array form synthesized transmitting signal and collect the return signal independently. The echoes of each sub-array are acquired at a different position along the flight path thus improving the

equivalent pulse repetition frequency and increasing the spatial sampling rate therefore achieving higher azimuth resolution and bandwidth. With M-channel system, azimuth resolution can be improved by M times.

1.3.7.   Inverse SAR: (ISAR)

This is a radar technique that utilizes the movement of a target while the illuminating sensor is stationary. ISAR mode uses radar imaging to generate a 2D high-resolution image of the moving target [7].

1.4.   Polarization of SAR signal

Unpolarized radar signal vibrates in all possible directions. SAR antenna sends and receives polarized signals in single plane perpendicular to the direction of propagation. The pulse of electromagnetic energy sent by the antenna may be horizontally or vertically polarized and these different polarizations determine physical properties of the target

1.5.   Backscatter

The antenna transmits the microwave signal and detects the backscattered signal in a sequential pattern. The backscattered signal provides information on phase, Doppler frequency, polarization, the time difference between pulse emission and return from the target, and magnitude or attenuation. The amplitude and phase of the backscattered signal depend on the roughness or geometry and permittivity of the target's surface [9]. The backscattered energy depends on the wavelength of the transmitted signal, angle of view, polarization and target's properties. Target properties such as roughness, governs the scattering pattern and the dielectric constant of the medium governs the strength of the backscatter. Urban buildings, dense vegetation, mountain slopes, wet soil, limestone, etc. have high backscatter while smooth surfaces like tarred or sandy roads, calm body of water, flooded soil, mud, etc. have little or no backscatter [1].
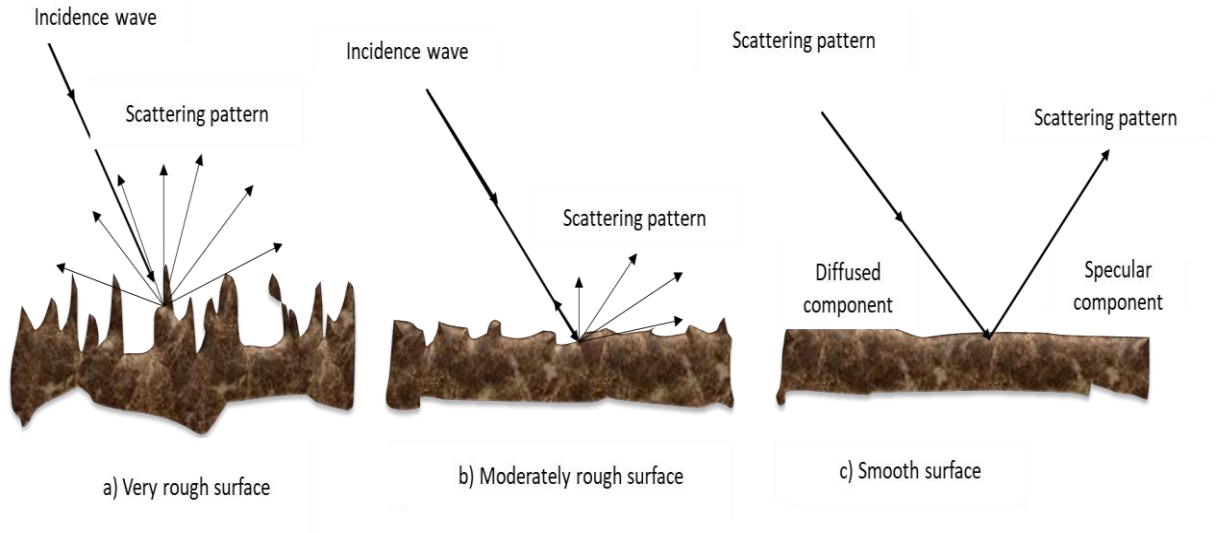
Figure 1.2. Surface scatter mechanism

1.5.1. Back scattering coefficients

Sigma Naught (σ^0), the backscattering coefficient sigma naught ($\sigma0$), is a normalized dimensionless number in dB that measures the backscattered signal strength [9]. It compares the backscattered signal strength to that expected from a square metre area.

Beta Naught (β^0), is the radar reflectivity (brightness) coefficient that does not depend on the local incident angle. The reflectivity per unit area in the slant range is dimensionless

Gamma (γ), the backscattered coefficient normalized by the cosine of the incident angle.

In the above-mentioned backscattering coefficients, sigma naught (σ^0) is widely used and preferred by most of the scientific communities.

σ^0 is related β^0 as : $\sigma^0 = \beta^0 \sin\alpha_i$, where α_i is the local incident angle.

1.6. Type of SAR Data.

SAR data consists of the high resolution backscatter energy from the target illuminated by modulated electromagnetic pulses from the radar sensor.

1.6.1. Raw Data

Raw Data (also known as level 0 product) are 2D data received directly from the SAR system. Raw data represent all the signals captured by the sensor from different targets. No information can be visualized since the raw data corresponds to a sensor whose azimuth and range resolutions are in several kilometers [12]. That is, raw data is uncompressed or unfocused (containing hundreds of rows and columns)

To perform specific SAR synthesis, Space agencies often provide raw data together with related processing information such as satellite telemetry.

Level 0 product are digitized on a low number of bits. For instance, ERS raw data are coded on 5 bits for imaginary and 5 bits for real part. Various techniques of compression of the level 0 product have been developed since the data have to transit from the SAR sensor to the receiver at the ground station fast and effectively with without significant losses [12].

1.6.2. Single-Look Complex Data (SLC)

SLC Data(image) is obtained by compressing the SAR raw data in range direction (pulse compression) and in azimuth direction (SAR synthesis). This image is a 2D table of complex data (pulse direction, radar track) related physically to the sensor. The image resulting from the processing of the 2D level 0 product is actually the first scientific product [12]. The range and azimuth compression algorithm is known as level 1.

Level zero products are processed by a PAF. Each Processing and Archiving Facility has its own signal processing algorithm for processing specific raw data. The data provided depends on how they have been processed. For this reason, it is advisable to use data from the same Processing and Archiving Facility for multi-data analysis.

1.6.3. Multi-look Data.

Space agencies usually provide precision images (images whose square pixels are based on ground geometry) for easier analysis and usable. Multi-look processing requires two major steps azimuth filtering (to enable reduction of speckle noise noted) and range over-

sampling (takes into account look angle variation along the swath). The resulting data after multi-look processing are amplitude value and are coded in 16-bits data [12].

1.6.4. Geocoded Data.

These are data relatively geocoded, that is dependent and geographically related to other reference points rather than sensor reference system as the case with SLC data. Georeferenced data are sometimes provided by space agencies and these data are North-South oriented.

1.6.5. Polarimetric Data.

Polarimetric data are multidimensional data and therefore its visualization is changing. Once existing polarimetric SARs such as AirSAR and SIR-C/X-SAR (2001) provide fully polarimetric data by transmitting and receiving signals of multipolarization.

2. PRINCIPLES OF RADAR OPERATION

The radar sensor encompasses all the electronics required to generates, transmits and receives SAR signals. These sensor electronics include a radar antenna, a data link, a recording device or physical interface to convey collected signals to the IFP. Basically, there are 7 components that comprise the radar sensor [13].

- The wave generator generates the waveform to be modulated. It provides three types of modulation techniques such as amplitude modulation(AM) and linear frequency modulation(LFM). Each modulation technique depends on a specific application.
- The Transmitter generates powerful electromagnetic pulses at a precise time interval and transmits to the antenna block through either a solid-state device or through resonating microwave tubes for transmission.
- The Antenna radiates the electromagnetic pulses generated from the transmitter in a beam. The returned echo energy picked up by the antenna follows another path to the receiver. For a monostatic system, an electronics switch (duplexer) is used to connects and disconnect the antenna from the transmitter and receiver when transmitting and when receiving a pulse.
- The Receiver receives the target reflected energy through the antenna, amplify, filter, and demodulate the received signal. The demodulated or digital signal is sent to the signal processor of the computer for further processing.
- The signal processor extract range information or target velocity by performing complex mathematical operation on the digital signal.

- The timing generator controls the operation of the radar components and enable synchronization of various signals by providing timing information. The targets' information's are sent out for display on cathode ray tube.

The figure 2.1. below shows the block diagram of a Pulse Linear Frequency Modulation radar system [13], [9].

The transmitter of PLFM radar sensor comprises of a pulse generator, a modulated signal generator, PA, mixer and local oscillator. The receiver is made up of LNA, mixer, demodulator local oscillator, A/D converter and signal processor. The antenna system is either connected to the receiver or the transmitter through a duplexer each at a time.
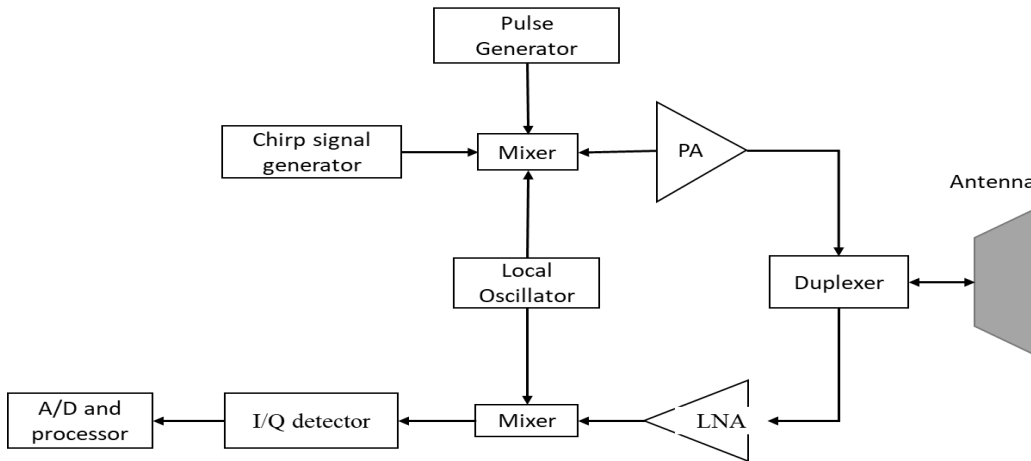
Figure 2.1. PLFM radar system

2.1.   Radar Modulation Techniques

Radars are able to determining the distance of an object from their sensors. They are also capable to determine the speed of a moving object. This can be done by timing the delay from when the chirp signal is transmitted to when the echo is received, or by determining the frequency difference between the transmitted signal and the received echo. The timing of pulse delay employs the AM technique while the detection of the frequency difference and ranging employ the linear FM technique [13].

2.1.1. Frequency Modulation Technique.

In this technique, the carrier frequency is varied in accordance with characteristics of the modulated (baseband) signal $S_b(t)$ [6], [13].

$$S(t) = A_0 \exp\left[j(\omega_C t + \alpha \int_{-\infty}^{t} S_b(t)dt) \right]$$

Since baseband-modulating signal $S_b(t)$, is normally a sinusoidal function, then

$$S(t) = A_0 \exp\left[j(\omega_C t + \alpha \int_{-\infty}^{t} \cos(2\pi f_a t)dt) \right]$$

$$= A_0 exp[j(2\pi f_C t + \alpha sin\omega_a t)] \tag{2.1}$$

Where α is modulation index or the maximum phase deviation value and f_c is the carrier frequency. By differentiating the instantaneous [13], [6], phase of S(t), we obtain the instantaneous frequency f, as

$$f = \frac{1}{2\pi} \frac{d}{dt} \left[w_c t + \alpha \int_{-\infty}^{t} S_b(t)dt \right] = f_c + \frac{1}{2\pi} \alpha S_b(t) \tag{2.2}$$

2.1.1.1. Linear FM (LFM) Technique.

The frequency of a transmitter is either increasing or decreasing continuously from the reference frequency [9]. The transmitted FM is modified in order to be linear with time.

From the instantaneous frequency [6] obtained in equation 2.2.

$$f = f_c + \frac{1}{2\pi} \alpha S_b(t)$$

$$f = f_c + k_r t, \quad \text{when } \alpha S_b(t) = 2\pi k_r t,$$

Where k_r is known as the chirp rate (frequency changing rate) [5], [9] and is given as,

$$k_r = {df}/{dt}$$

Therefore $S(t) = A_0 \exp\left[j(\omega_c t + \alpha \int_{-\infty}^{t} S_b(t)dt) \right] = A_0 \exp\left[j(\omega_c t + \int_{-\infty}^{t} 2\pi k_r t dt \right]$

$$S(t) = A_0 \exp(j2\pi f_c t + j\pi k_r t^2) \tag{2.3}$$

15

There are two common forms of LFM used in radar application: the chirp or the Pulsed LFM and the continuous-wave LFM.

2.1.1.2.   Pulsed LFM Technique

Lets $p_1(t)$ be defined as

$$p_1(t) = Rec\left(\frac{t - {}^{\tau_p}/_2}{\tau_p}\right)$$

Where the rectangular rect(t) [10], [13] is defined [6], [13], [10]as

$$rect(t) = \begin{cases} 1, & |t| \leq \frac{1}{2} \\ 0, & |t| > \frac{1}{2} \end{cases},$$

and let $p_2(t) = A_0 \exp[j(2\pi f_c t + \pi k_r t^2)]$

The Pulsed symmetrical LFM signal S(t) with pulse duration τ_p is gotten as follows;

$$S(t) = p_1(t).p_2\left(t - {}^{\tau_P}/_2\right)$$

$$= Rec\left(\frac{t - {}^{\tau_p}/_2}{\tau_p}\right).A_0 \exp\left(j2\pi f_c\left(t - {}^{\tau_p}/_2\right) + j\pi k_r\left(t - {}^{\tau_p}/_2\right)^2\right) \quad (2.4)$$

and the Pulsed nonsymmetrical LFM signal S(t) with pulse duration τ_p as;

$$S(t) = p_1(t).p_2(t)$$

$$= Rec\left(\frac{t - {}^{\tau_p}/_2}{\tau_p}\right).A_0 \exp(j2\pi f_c t + j\pi k_r t^2) \quad (2.5)$$

The figures below show the time–frequency relation of a pulsed LFM [13]

The pulsed LFM waveform has pulse duration time τ_p where $f_{max} = k_r\tau_p$ and the frequency bandwidth is

$$B = f_{max} = k_r\tau_p \quad (2.6)$$

16

(a) Pulse sequence

(b) pulsed LFM signal Waveform
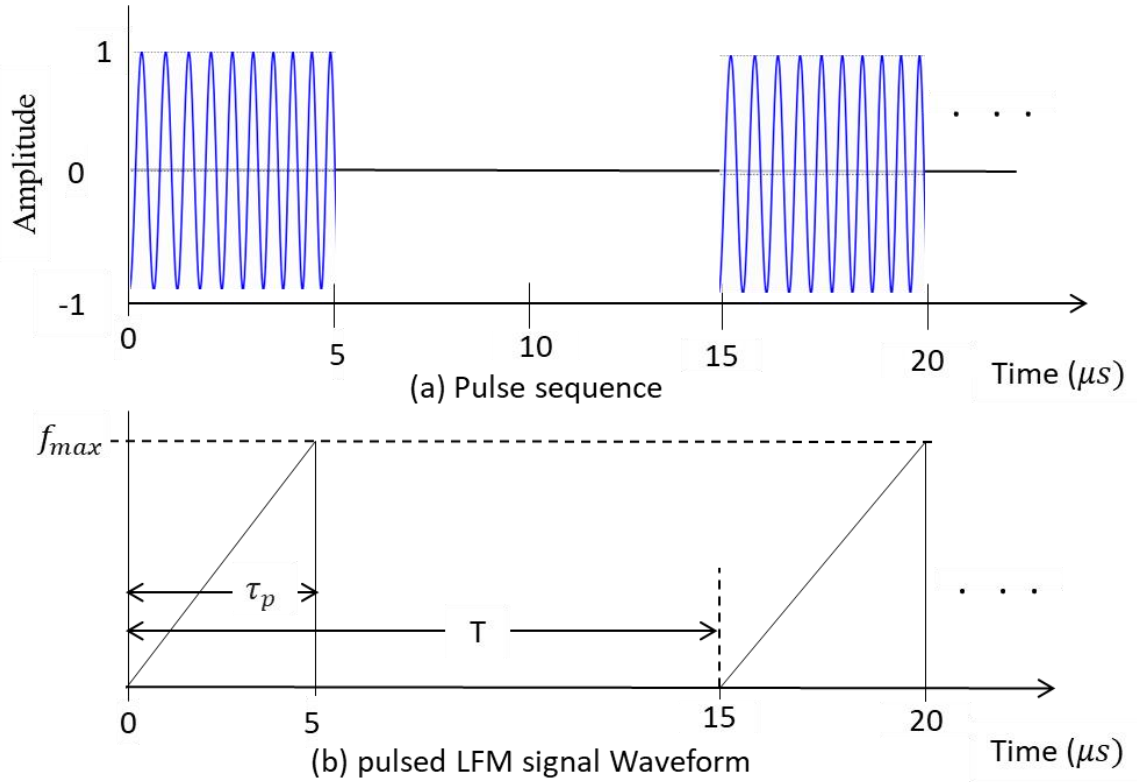
Figure 2.2. Lear FM pulsed train

2.1.2. The Frequency Spectrum of LFM-Based Signals

Considering the $p_1(t)$ and $p_2(t)$ mentioned above. The Fourier transform of $p_1(t)$ and $p_1(t)$ is $P_1(f)$ and $P_2(f)$

Frequency spectrum of a nonsymmetrical LFM signal S(t) is obtained by convolving spectra $P_1(f)$ and $P_2(f)$. That is,

$$P_1(f) = \mathcal{F}\{p_1(t)\}$$

$$= \mathrm{T}.\frac{\sin(\pi f \boldsymbol{\tau_p})}{\pi f T_p}.\exp(j\pi f \boldsymbol{\tau_p})$$

$$= T.sinc(f\boldsymbol{\tau_p}).\exp(j\pi f \boldsymbol{\tau_p})$$

and $P_2(f) = \mathcal{F}\{p_2(t)\}$

17

$$= \int_{-\infty}^{\infty} exp\{-j(2\pi f_c t + \pi k t^2\}. exp(-j2\pi ft)dt$$

$$= \int_{-\infty}^{\infty} exp\left[j\pi k_r \left\{\left(t - \frac{f-f_c}{k_r}\right)^2 - \frac{(f-f_c)^2}{k_r^2}\right\}\right]dt$$

$$= exp\left\{-j\pi \frac{(f-f_c)^2}{k_r}\right\}. \frac{1}{\sqrt{\pi}} \int_{-\infty}^{\infty} exp(jk_r x^2)\, dx,$$

where $x = \sqrt{\pi}\left(t - \frac{f-f_c}{k_r}\right).$

$$\int_{-\infty}^{\infty} exp(jk_r x^2)\, dx =?$$

Let $-v^2 = jkx^2$, then $dv = \sqrt{-jk_r}dx \rightarrow dx = \frac{dv}{\sqrt{-jk_r}}$

Then, $\quad \int_{-\infty}^{\infty} exp(jk_r x^2)\, dx = \frac{1}{\sqrt{-jk_r}} \int_{-\infty}^{\infty} exp(-v^2)\, dv = \sqrt{\frac{\pi}{k_r}} exp\left(j\frac{\pi}{4}\right).$

Therefore,

$$P_2(f) = exp\left\{-j\pi \frac{(f-f_c)^2}{k_r}\right\}. \frac{1}{\sqrt{\pi}} \sqrt{\frac{\pi}{k_r}} exp\left(j\frac{\pi}{4}\right)$$

$$= exp\left(j\frac{\pi}{4}\right). \frac{1}{\sqrt{k_r}} exp\left\{-j\pi \frac{(f-f_c)^2}{k_r}\right\}$$

$$S_T(f) = P_1(f) \otimes P_2(f),$$

where $\otimes$ represent the convolution

$$S_T(f) = T.sinc(f\tau_p). exp(j\pi f\tau_p) \otimes exp\left(j\frac{\pi}{4}\right). \frac{1}{\sqrt{k_r}} exp\left\{-j\pi \frac{(f-f_c)^2}{k_r}\right\} \qquad (2.7)$$

Practically, the frequency spectrum of LF signals are obtained by the application of DFT on the signal [9].

2.2. Target Detection of FM Based Radars

2.2.1. LFM Radar Detection Techniques.

The pulsed LFM signal S(t) with time [13] duration τ_p given as:

$$S(t) = A_0 \exp(j2\pi f_c t + j\pi k t^2)$$

Assuming an ideal target with amplitude A_0, is 1 then the received signal $S_r(t)$ can be written as:

$$S_r(t) = \sum_i exp[j2\pi f_c(t - t_i) + j\pi k(t - t_i)^2]$$

$$= \sum_i exp[j2\pi f_c(t - t_i)]exp[\pi k(t - t_i)^2]$$

$$= \sum_i exp[j2\pi f_c(t - t_i)]exp[\pi k t^2 - 2\pi k t_i t + \pi k t_i^2] \qquad (2.8)$$

Where t_i is the round trip time of the echo from ith target given as

$$t_i = \frac{2R_i}{c} \qquad (2.9)$$

Dechirp of the received signal $S_r(t)$ is done by multiplying the complex conjugate $S^*(t)$ of the received signal with the generated chirp signal. This complex conjugate $S^*(t)$ and the transmitting chirp signal S(t) are the same but complex conjugate $S^*(t)$ is continuous LFM signal with greater bandwidth [13]. The dechirped signal $S_c(t)$:

$$S_c(t) = S^*(t)S(t)$$

$$= S^*(t) \exp(j2\pi f_c t + j\pi k t^2) \quad , \ A_0 = 1$$

$$= \sum_i exp(j2\pi f_c t_i - j\pi k t_i^2)exp(j2\pi k t_i t) \qquad (2.10)$$

The dechirped frequency component $k t_i$ also known as beat frequency, carries information on the round-trip delay t_i.

Figure 2.3 shows the diagram of dechirp processing.
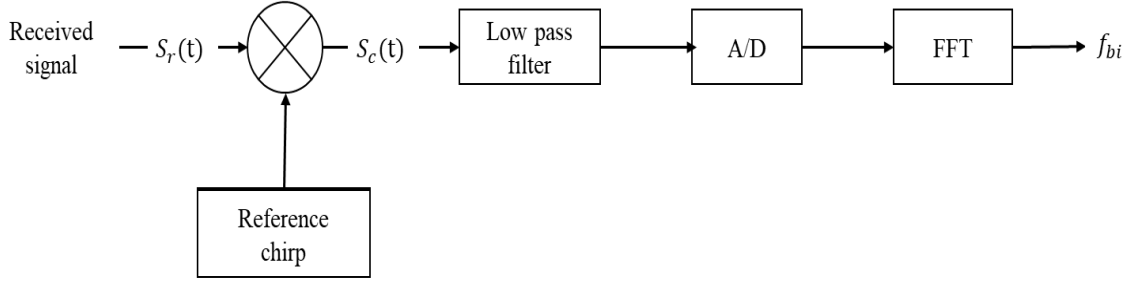
Figure 2.3. Diagram of dechirp processing.

The target range is obtained as;

$$R_i = \frac{cf_{bi}}{2k} \tag{2.11}$$

2.2.2. Quadrature Demodulator

Considering the LFM signal

$$S(t) = A_0 exp(j2\pi f_c t + j\pi k t^2)$$

The real value of the signal is represented as

$$S(t) = A_0 \cos(2\pi f_c t + \pi k t^2)$$

$$= \boldsymbol{A_0 \cos(2\pi f_c t + \emptyset(t))} \tag{2.12}$$

Where $\emptyset(t) = \pi k t^2$ is the phase term presented for illustration purposes. The carrier frequency f_c generally has a higher value as compared to kt. The time varying-phase $\emptyset(t)$ information is transmitted using the complex-valued signal [14], [13]. After transmitting the time-varying phase $\emptyset(t)$, information, the Quadrature demodulator is then used to acquire the correct phase information. As illustrated on figure 2.4 the in-phase–quadrature-phase demodulator splits any complex-valued LFM signal $s(t)$, into the real or in-phase (I), and imaginary or quadrature-phase Q, components of $\emptyset(t)$. Two carriers $\cos(2\pi f_c t)$ and $\sin(2\pi f_c t)$ are locally generated by the system. The LPF filter out high frequency component $4\pi f_c t + \emptyset(t)$ and retain the low-frequency component $\emptyset(t)$. The A/D converter digitizes the real and imaginary parts of the low frequency phase signal

20

$\emptyset(t)$ to obtain a complex number pair that serves as a row element of the two dimensional image the radar data [13], [7].
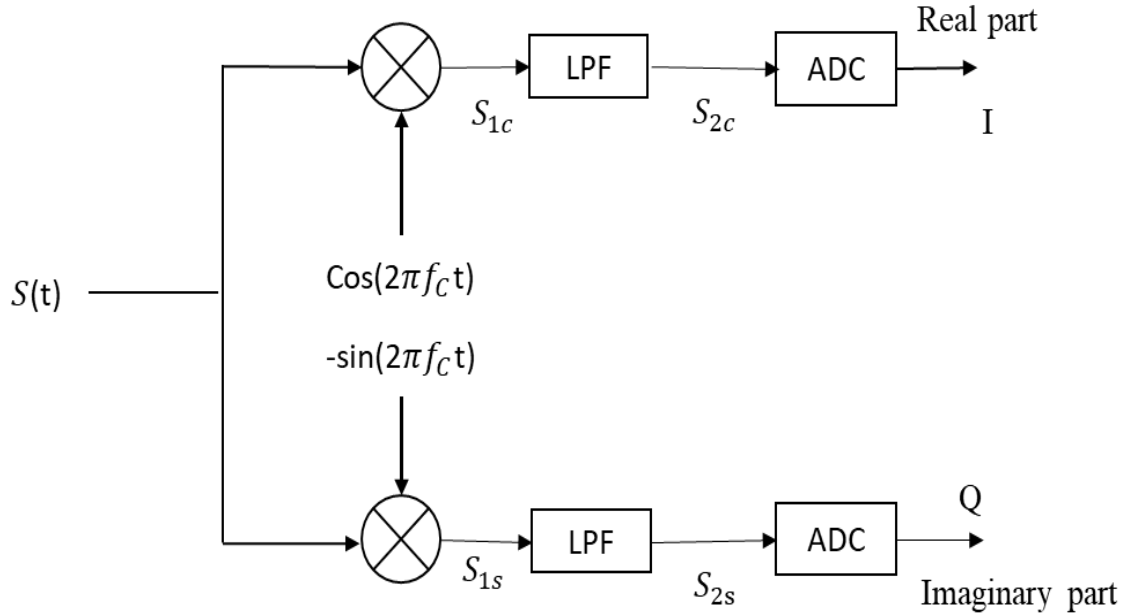
Figure 2.4. Quadrature demodulator

The following intermediate signals S_{1s}, S_{1c}, S_{2s} and S_{2c} are obtained as follows:

$$S_{1c}(t) = \frac{1}{2}\left(\cos(4\pi f_c t + \emptyset(t)) + \cos(\emptyset(t))\right),$$

$$S_{1s}(t) = \frac{1}{2}\left(\sin(4\pi f_c t + \emptyset(t)) + sin\emptyset(t)\right),$$

$$S_{2c}(t) = \frac{1}{2}\cos(\emptyset(t)),$$

$$S_{2s}(t) = \frac{1}{2}\sin(\emptyset(t)).$$

The time varying signal phase $\emptyset(t)$ can then be obtained as:

$$\boldsymbol{\emptyset(t) = \tan^{-1}\left(\frac{S_{2s}(t)}{S_{2c}(t)}\right)} \tag{2.13}$$

21

2.2.3. Matched Filtering (Pulse Compression) Technique

Matched filtering is a technique used to regain a signal that was corrupted by additive white Gaussian noise. A matched filter is applied on received signal in order to identify a target by determining whether the filter output (compressed pulse), exceeds a specific threshold. Different targets produce pulses of different magnitudes and each magnitude depends on three factors: targets reflectivity (σ), pulse width (τ_p) and range (R) from the radar sensor to target. The effective width of a compressed pulse is determined by the bandwidth and the pulse width τ_p of the received signal

Considering an ideal target with [13] reflectivity 1 and zero signal attenuation [13] between the radar sensor and target area. If the input signal is x*(t)* and the Fourier transform of the input signal is X *(f)*, then the matched [15], filter $h(t)$ and the Fourier transform of the matched filter $H(f)$ can be expressed as follows:

$$h(t) = x^*(t) \quad \text{and} \quad H(f) = X^*(f)$$

If *f(t)* is the output of the matched filter, then

$$F(f) = X(f)H(f) = |X(f)|^2$$

Therefore
$$f(t) = F^{-1}(|X(f)|^2) = x(t) * h(t) = \int x(\tau)h(t-\tau)d\tau$$

$$f(t) = \int x(\tau)h(t-\tau)d\tau$$

For h(t)=x^*(t) , then,

$$f(t) = \int x(\tau)x^*(t+\tau)d\tau \ .$$

This is the definition of autocorrelation of x(t). That is the matched filtering of any signal x*(t)* is equivalent to the autocorrelation of that signal x*(t)* with itself.

Consider the echo of a nonsymmetric LFM signal *S(t)* to be the echo signal from single target:

$$S(t) = Rec\left(\frac{t-\tau_p/2}{\tau_p}\right).A_0\exp(j2\pi f_c t + j\pi k t^2)$$

If $A_0 = 1$ and $h\ (t) = x^*(t)$, then the output of the matched filter is given as:

$$f(t) = \int_0^{\tau_p} s(\tau)s^*(t + \tau)d\tau$$

$$= \int_0^{\tau_p} \exp(j2\pi f_c\tau + j\pi k\tau^2).\exp\{-j[2\pi f_c(t + \tau) + j\pi k(t + \tau)^2]\}$$

$$= \left[-j\left(2\pi f_c t + \pi k t\tau_p + \pi k t^2\right)\right].T.\frac{\sin(\pi k t\tau_p)}{\pi k t\tau_p} \tag{2.14}$$

The signal bandwidth $B = k\tau_p$, so $kt\tau_p = Bt$, let $z = kt\tau_p$, then

$$|f(z)| = \tau_p.\frac{\sin\pi z}{\pi z} = \tau_p.sinc(z).$$

$|f(z)| = \tau_p$ when $z = 0$, that is $|f(z)|$ has a maximum value of τ_p when $z = 0$

At $z = 1$, $\text{sinc}(z) = 0$, or $z = Bt = 1$, $t = {}^1\!/_B$.

It is also true that for sinc(z) function, the 3-dB mainlobe width (compressed pulse width) is equal to the first z value of which sinc(z) = 0. Therefore 3-dB mainlobe width is $\frac{1}{B}$, where the bandwidth of a LFM signal B is $k\tau_p$ with pulse width time τ_p

Therefore the pulse compression ratio$= \frac{Original\ LFM\ pulse\ duration}{Compressed\ pulse\ duration}$

$$= \frac{\tau_p}{{}^1\!/_B} = B\tau_p \tag{2.15}$$

Where $B\tau_p$ is the time bandwidth product.

Since convolving of two signals in the time domain is same as multiplying the two signals in the frequency domain, therefore, the matched filter will be implemented by first transforming the received signal and the matched filter function into frequency domain using Fast Fourier Transform. The resulting product of the frequency domain functions are then converted back to time domain by applying Inverse Fast Fourier Transform. Matched filter function is shorter than the received signal because of different ranges of different targets. For this reason, paddings with zeros on the matched filter function is

23

required when applying the Fast Fourier Transform on the matched [13] filtering. Figure 2.5 below shows the block diagram of DFT-based pulse compression process.
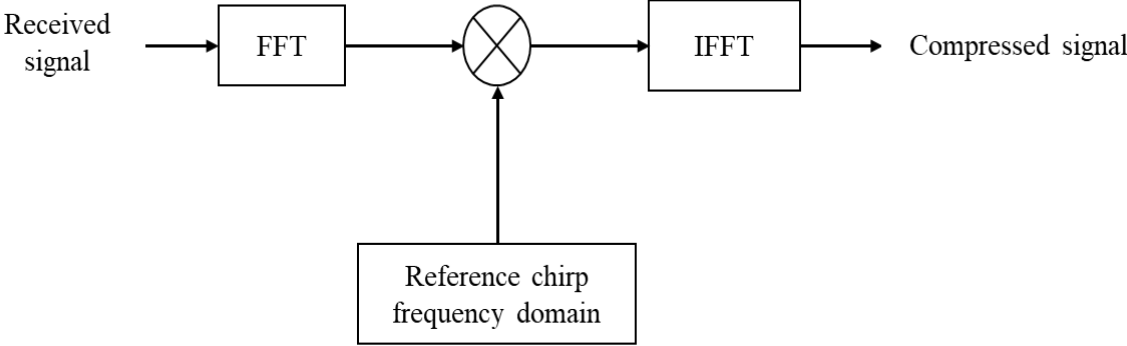
Figure 2.5. Block diagram of DFT-based pulse compression

3.   SAR IMAGING GEOMETRY

Generally, synthetic aperture radar is a pulse radar system. Figure 3.1. shows and imaging side looking monostatic satellite with radar sensor onboard with an antenna of length L_a and width w_a, oriented parallel to the flight direction. The satellite moves in a flight trajectory (azimuth) at a constant velocity V at an altitude h above the ground. During flight, the radar sensor transmits [13] chirp signals and receive target echoes from the ground swath. The pulse is directed at look angle θ (fixed side looking direction) at certain pulse repetition frequency, f_{PRF} with pulse width time τ_p. The pulse is repeated at the pulse repetition interval, $T = {1}/{f_{PRF}}$, where T is the period from the start of one pulse to the start of the next pulse. The target distance from the radar sensor is known as the slant range denoted R_0. The 3-dB bandwidth of the chirp signal along the azimuth track is given as $B_{az} = {\lambda}/{L_a}$ and along the [15] range track is $B_r = {\lambda}/{w_a}$. λ is the wavelength of the chirp signal. The duration, ΔT_p at which the pulse illuminate the target is $R_0\left(\frac{B_{az}}{V}\right)$.

The echoes from targets at the same slant range will arrive the sensor same time. The radar image is formed in azimuth and slant range coordinates. Targets at the same slant range differ only in Doppler frequency due to the radial velocity difference of the radar relative to target. For broadside-mode SAR, the two axes of elliptically shaped beam footprint can be determined by $R_0 B_{az} = R_0\,{\lambda}/{L_a}$ and $R_0 B_r = R_0\,{\lambda}/{w_a}$ respectively while for squint-mode SAR, all the parameters are the same as in broadside-mode SAR but for the angle φ which the beam form with the nonzero squint angle.
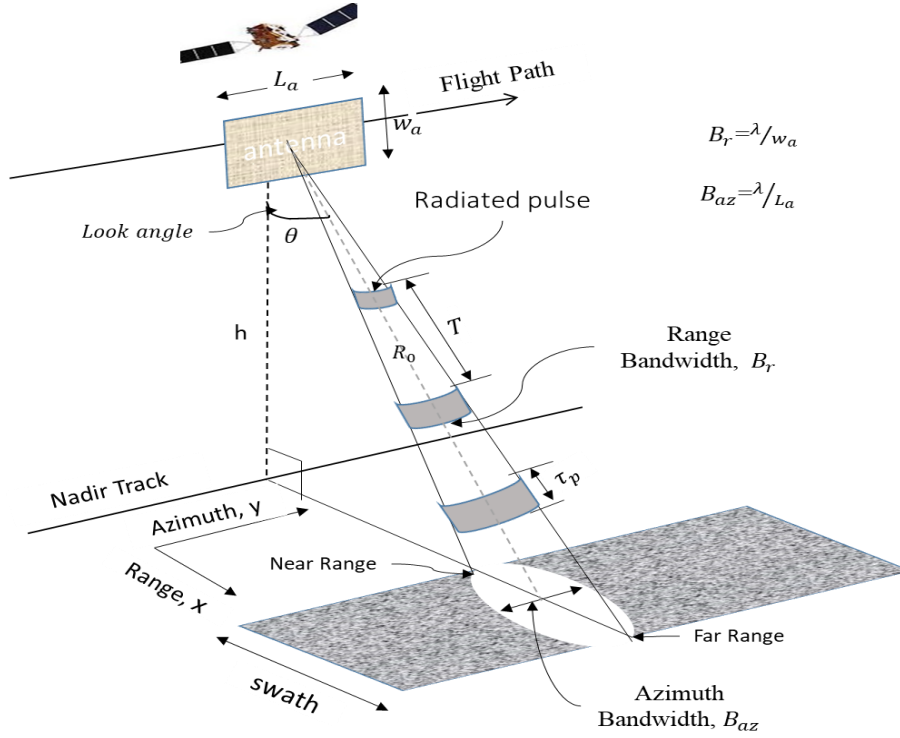
Figure 3.1. Stripmap imaging radar geometry.

3.1. SAR Raw data generation

From equation 2.5, the PLFM radar waveform [6], [13], [10],

$$S(t) = Rec\left(\frac{t - {}^{\tau_p}/_2}{\tau_p}\right).A_0 exp(j2\pi f_c t + j\pi k_r t^2)$$

With a rectangular gate function $Rec\left(\frac{t}{\tau_p}\right)$, pulse duration time τ_p, amplitude of transmitted signal A_0, and PLFM chirp rate k_r. The chirp signal starts and end at $t = 0$ and τ_p respectively.

Let suppose the gate function is $\alpha(t)$ and the amplitude A_0 as 1. Considering the echoes are from I different reflectors, with reflective coefficient σ_i corresponding to ranges R_i, where $i = 1, 2, 3, \ldots, I$, then the signal S(t) written as the sum of delayed echoes [13]is

26

$$S(t) = \sum_{i=1}^{I} \sigma_i \alpha(t - \frac{2R_i}{c}) \; .exp\left\{ j2\pi f_c \left(t - \frac{2R_i}{c} \right) + j\pi k_r \left(t - \frac{2R_i}{c} \right)^2 \right\}$$

$$= \sum_{i=1}^{I} \sigma_i \alpha(t - \tau_i) \; .exp\{ j2\pi f_c(t - \tau_i) + j\pi k_r(t - \tau_i)^2 \} \tag{3.1}$$

Where $\tau_i = \frac{2R_i}{c}$ is the echo delay time from the ith target. Considering that the target location at any point $(x_i, \; y_i)$ with radar the position at $(0, \; 0)$ at an altitude 0, then τ_i can be calculated as:

$$\tau_i = 2\left(\frac{R_i}{c}\right) = 2\left(\frac{\sqrt{x_i^2 + y_i^2}}{c} \right).$$

And the range is calculated as:

$$R_i = \frac{1}{2}(c\tau_i)$$

The baseband signal $S_b(t)$ can be obtained through the quadrature demodulation process by first removing the frequency of the carrier and applying a low pass filter (LPF). The demodulated baseband signal can be obtained as:

$$S_b(t) = \sum_{i=1}^{I} \sigma_i |\alpha(t - \tau_i)|^2 \; exp\{ -j2\pi f_c\tau_i + j\pi k_r(t - \tau_i)^2 \}$$

If η is the time index of the demodulated signal, then the baseband signal $S_b(t)$ can be express in terms of n as:

$$S_b(t_\eta) = \sum_{i=1}^{I} \sigma_i |\alpha(t_\eta - \tau_i)|^2 \; \exp\left\{ -j2\pi f_c\tau_i + j\pi k_r\left(t_\eta - \tau_i\right)^2 \right\} \tag{3.2}$$

with $\eta = 0,1,2, \ldots, N-1$. Where N is the total number of range samples receive. N is a function pulse duration time, number of targets, and sampling frequency. The signal in 3.2. is based on a single pulse duration transmitted from a single position. Suppose the radar is moving along the azimuth direction (direction perpendicular to the radar beam) emitting signal at pulse repetition frequency f_{PRF}, then a two dimensional received data array will be obtain.

Suppose the moving radar position along the azimuth is u_m, where $m = 1, 2, 3,$ $\ldots, M.$ with M as the total number of processed azimuth lines and must be greater than or equal to the number of azimuth lines (N_{az}) within the length L_s (synthetic aperture).

Therefore, 3.2. written in 2D is:

$$S_b(u_m, t_\eta) = \sum_{i=0}^{I} \sigma_i |\alpha(t_\eta - \tau_{umi})|^2 \exp\left\{-j2\pi f_c \tau_{umi} + j\pi k_r(t_\eta - \tau_{umi})^2\right\} \quad (3.3)$$

Where $\tau_{um,i} = 2\left(\frac{R_{umi}}{c}\right)$ is the received signal delay time from the ith target with radar located at the position u_m.

3.2.   System model for generation of broadside SAR image

Figure 3.2. shows a broadside SAR system model used to generate a 2D SAR image. In this model, the altitude of the radar is considered to be zero that is $h = 0$, and the radar moving at the speed V along the flight path or y-axis. The 3-dB bandwidth along the flight path is denoted B_a. The radar [13], center beam in broadside SAR system is always perpendicular to the flight path. The three targets are located at (R_{0a}, u_1), (R_{0b}, u_2) and (R_{0a}, u_3) respectively where u_1, u_2, u_3 are radar positions corresponding to the position where the targets are illuminated [16] under the center beam. The synthetic aperture lengths $L_{sa} = R_{0a}B_a$ and $L_{sb} = R_{0b}B_a$ correspond to targets at range R_{0a} and R_{0b} respectively. The total synthetic aperture length $L_{s\,total}$, of the three targets is calculated as

$$L_{s\,total} = L_{sa} + (u_3 - u_1) \qquad (3.4)$$
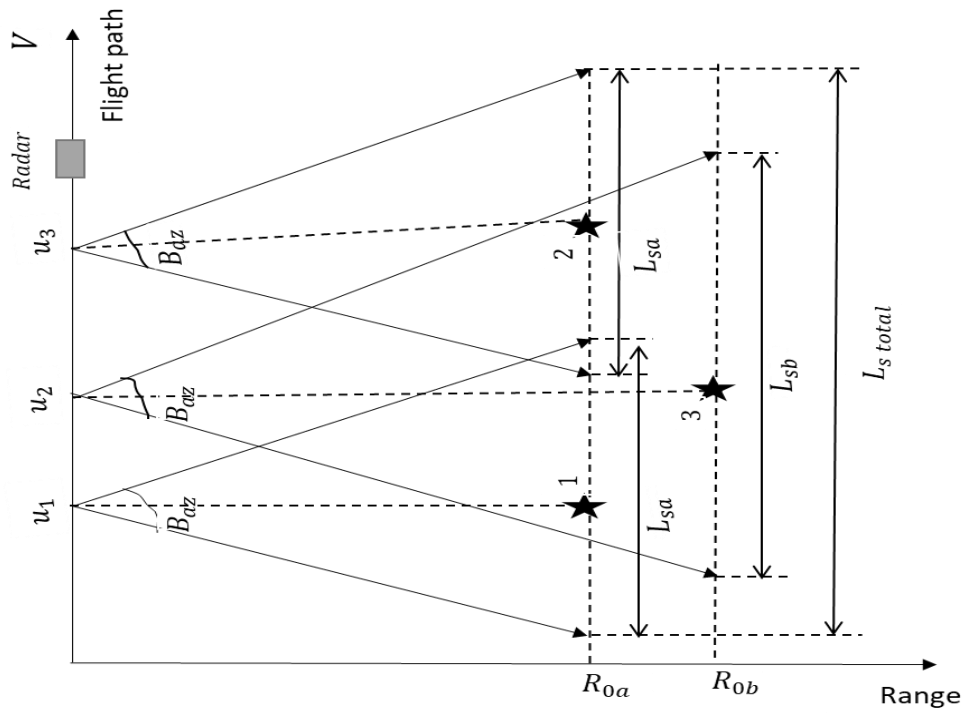
Figure 3.2. A 2D model of a broadside SAR system image generation

In order to simplify the broadside SAR system model above for radar image generation, three assumptions were made.

- The target is assumed to be an ideal stationary reflector so that motion compensation should not be required.
- The inclination angle effect is ignored as the slant range is considered equal to the ground range
- The background objects were ignored so that the acquire signal is noiseless.

3.3. System model for generation of squint SAR image.

Figure 3.3 shows a 2D squint SAR system model for radar image generation. The squint angle φ is the angle between the radar center beam and the range axis.
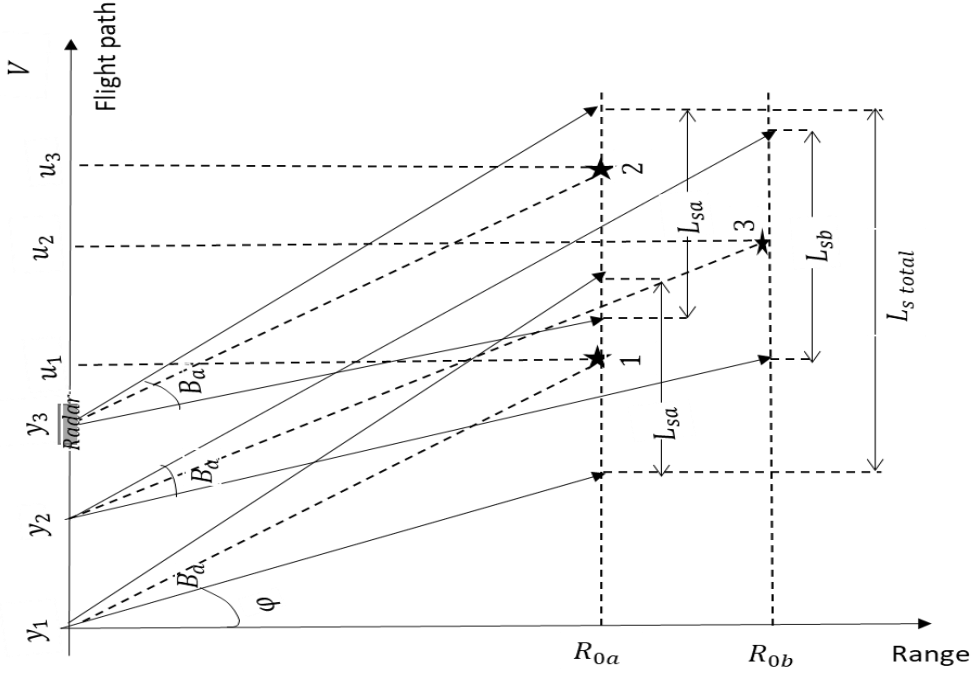
Figure 3.3. A 2D squint SAR system model for radar image generation

The location of the three targets are (R_{0a}, u_1), (R_{0b}, u_2) and (R_{0a}, u_3) respectively. The radar synthetic aperture [13] lengths L_{sa} and L_{sb} corresponding to the targets ranges R_{0a} and R_{0b} are expressed respectively as:

$$L_{sa} = R_{0a}[tan(\varphi + 0.5B_a) - tan(\varphi - 0.5B_a)]$$

$$L_{sb} = R_{0b}[tan(\varphi + 0.5B_a) - tan(\varphi - 0.5B_a)]$$

The total synthetic aperture length L_{stotal}, for the three targets is

$$L_{stotal} = L_{sa} + (u_3 - u_1) \tag{3.5}$$

3.4.   Image data array synthesis of a broadside SAR system

The figure 3.4. below shows a model of broadside SAR image generation from a target response with target location at (R_0, u_2). The three radar positions u_1, u_2 and u_3 are positions where the radar beam starts and ends to illuminating the target respectively. The

slant ranges R_1, R_2 and R_3 correspond to [6], [16] the locations of the radar respectively at $(0, u_1)$, $(0, u_2)$ and $(0, u_3)$.
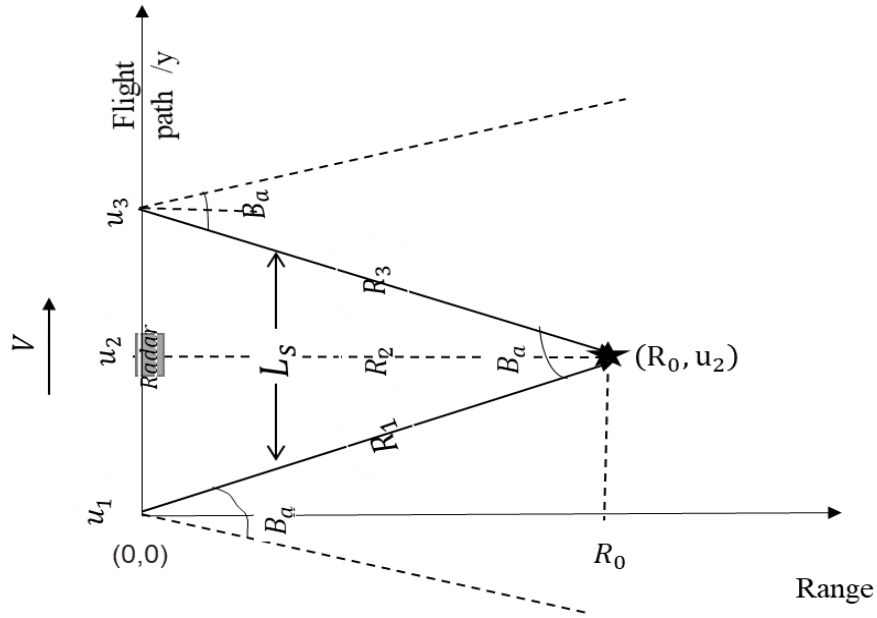
Figure 3.4. A broadside SAR system model for a single-target radar image generation

The model of the received signal array of the broadside SAR in figure 3.4 is displayed on figure 3.5 below. The azimuth samples are represented by the m-axis (y-axis) and the delay time of the radar echo from the target is represented by the t-axis (x-axis). The position of the radar corresponds to each line (azimuth sample) on figure. There are total of N_{az} number of lines or azimuths samples within the synthetic aperture length L_s. The total number of lines N_{az} is equal to the ratio of the synthetic aperture length L_s to the sample spacing A_s. That is:

$$N_{az} = {L_s}/{A_s}$$

The azimuth locations m = 1 and m =N_{az} correspond to the radar positions where the beam starts and ends illuminating the target respectively. The mid position $m = {N_{az}}/{2}$ corresponds to the position where the target is under the radar center beam.

31
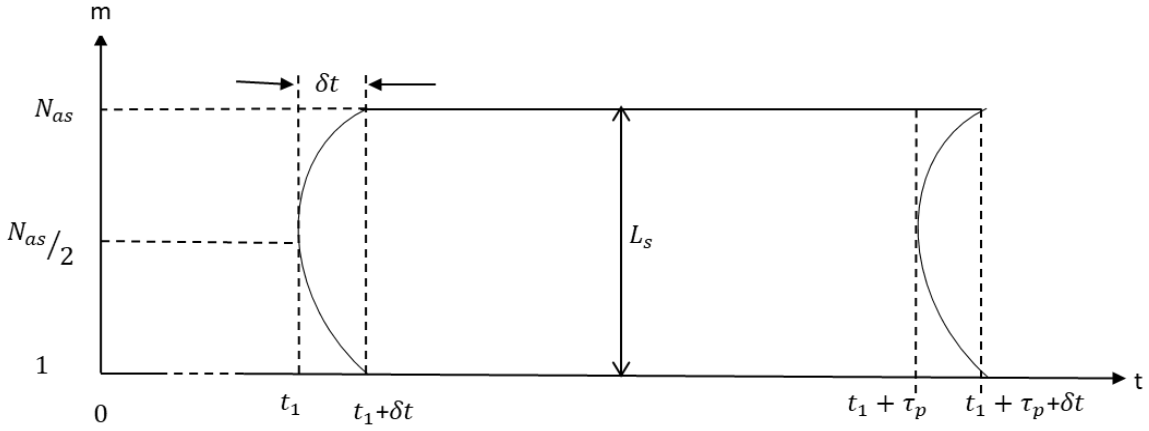
Figure 3.5. The received signal array of the broadside SAR in figure 3.4

The time t_1 to $t_1 + \tau_p + \delta t$ is the time when the pulse return to the radar. The closed target reflection time t_1 is expressed as:

$$t_1 = \frac{2R_0}{c} = \frac{2R_2}{c}$$

The time difference δt between the echoes or center radar beam and the two edges of the 3-dB radar beam width is calculated as;

$$\delta t = \frac{2}{c}(R_1 - R_2) = \frac{2}{c}(R_3 - R_2)$$

The slant range sample n_s and the time sample n_t are given as:

$$n_t = \frac{t}{\Delta t} = tf_s$$

$$n_s = \frac{R}{R_s} = R\left(\frac{f_s}{c}\right)$$

Where f_s is the sampling frequency and R and R_s are the slant range and slant range sample spacing respectively. The time t, and slant range R, are related as:

$$t = \frac{2R}{c}$$

Also the time sample n_t and the slant range sample n_s are related as:

$$n_t = 2n_s$$

32

A simplified and digitalized plot of figure 3.5 is displayed in figure 3.6. where the time axis is replaced with n_t (time sample). For convenient of study, let $n_t = 1$, and $n = N_r$, be the starts at $t = t_1$ and ends at $n = N_r$ respectively, with N_r the integer of $(\tau_p f_s)$, τ_P is the pulse duration time.
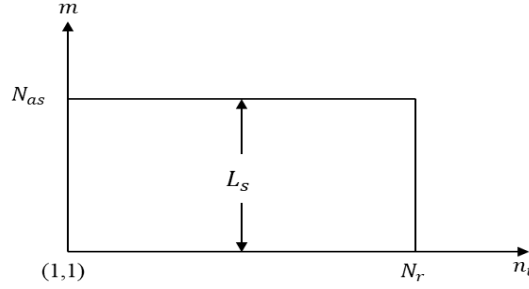
Figure 3.6. Simplified and digitalized received signal array of figure 3.5

The baseband echo signal from a single target with an amplitude of 1 and reflective coefficient 1 can then be expressed as follows,

$$S_b(u_{m,}\, t_\eta) = \exp\left\{-j2\pi f_c \tau_{u_m} + j\pi k_r (t_\eta - \tau_{u_m})^2\right\} \tag{3.6}$$

For a radar at point $(0, u_m)$, with a target located at (R_0, y_1) the delay time of echo τ_{u_m}, is obtained as

$$\tau_{u_m} = \frac{2}{c}\left(\sqrt{(u_m - y_1)^2 + R_0^2}\right) \tag{3.7}$$

3.5. Synthesis of a Squint SAR image data array

The image generation model of a squint SAR from a single target located at $(R_0, 0)$ is shown on figure 3.7. The three radar positions u_1, u_2 and u_3 is where the radar beam starts illuminating in the center and ends illuminating the target respectively. The slant ranges R_1, R_2 and R_3 corresponds to the radar located at $(0, u_1)$, $(0, u_2)$ and $(0, u_3)$ respectively. The angle φ between the radar center beam and the range axis and when the radar is at $(0, u_2)$ is the squint angle.

33

Figure 3.7. Single-target squint SAR System model.

The relationship between the time–azimuth of the received signal array is displayed on figure 3.8, where the vertical and horizontal axes shows the positions of the radar and the return time of echo signal respectively.

Figure 3.8. A received signal array from figure 3.7.

34

In this case, the SAR received signal array appears as a parallelogram where the longest time for echo to arrive at radar position u_1 is $t_1 = 2\left(\frac{R_1}{c}\right)$ and the shortest time for echo to arrive at radar position u_3 is $t_3 = 2\left(\frac{R_3}{c}\right)$. The echo arrived the radar position u_2 between the time t_1 and t_3.

A simplified plot of figure 3.8. is shown in figure 3.9. The azimuth sample is replaced with the radar position u and the time sample n_t replaces the time t.
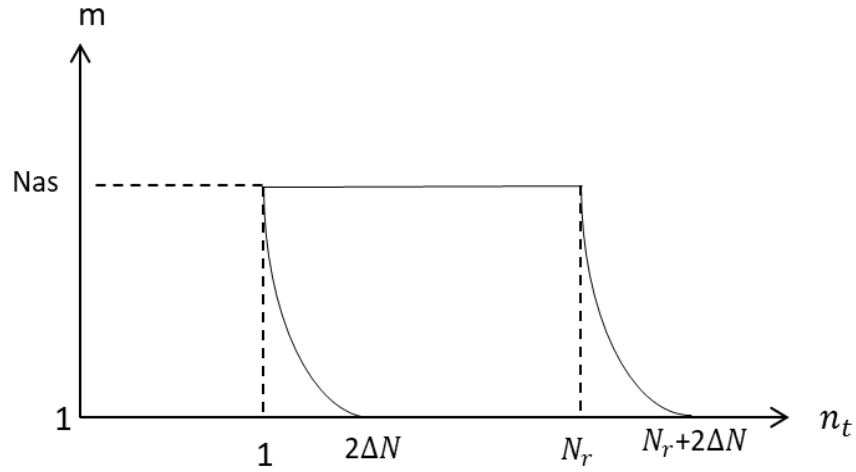
Figure 3.9. A digitalized signal array from figure 3-9

Synthetic aperture length, $L_s = R_0[tan(\varphi + 0.5B_a) - tan(\varphi - 0.5B_a)]$

Longest slant range $R_1 = R_0/cos(\varphi + 0.5B_a)$
Shortest slant range $R_3 = R_0/cos(\varphi - 0.5B_a)$
The maximum range migration amount $N = (R_1 - R_3)/R_s$
In squint SAR system, range migration occurs if $R_1 - R_3 > {}^1/_4$ of sample spacing or range resolution. That is range migration occurs if $R_1 - R_3 > \frac{1}{4}\left(\frac{c}{2B}\right)$, and therefore, range migration correction is needed.

With the assumptions above, the squint SAR baseband signal array can be derived based on the waveform of 3.3.

4. SAR SYNTHESIS ALGORITHMS

The received 2D data array synthesized from the waveform of 3.3 has a waveform of size M by N in both azimuth and the range (time) directions. The 2D data array is formed by M bursts of the radar pulse with N samples each. The data spread in range is caused by the time duration of the transmitted PLFM signal while the spread in azimuth is due to the fact that the target is under illumination by the radar beam during which the radar is collecting echoes in a period which the [16] radar covers the synthetic aperture length L_s.

The main aim of processing raw data is to convert it into a single pixel in the final processing stage. There exist a number of SAR signal processing techniques. Each and every SAR signal processing technique has its advantages and disadvantages. Some of these SAR signal processing techniques which are based on matched filters include; Range-Doppler, Wave domain, Omega-K, Chirp Scaling, Spectral Analysis, Stolt interpolation. The Range-Doppler technique, the Stolt-interpolation technique and the Chirp scaling technique are implemented and discussed in this work. Each of these techniques has its own advantages in high-quality imaging or computation efficiency. For instance, the Range-Doppler technique is an accurate approximation and computationally efficient for processing radar images while Stolt interpolation technique is computationally intensive, but has advantages over the Range-Doppler technique.

4.1. Range Doppler technique for processing of SAR signal.

There are three major tasks when processing SAR data by implemented the typical Range-Doppler processor: firstly, the range compression, followed by the cell migration correction, and lastly the azimuth compression. The range Doppler technique [17], [16]is

displayed in figure 4.1. The 2D raw data (complex data) refers to the quadrature demodulated baseband signal. The range compression is done in three steps.
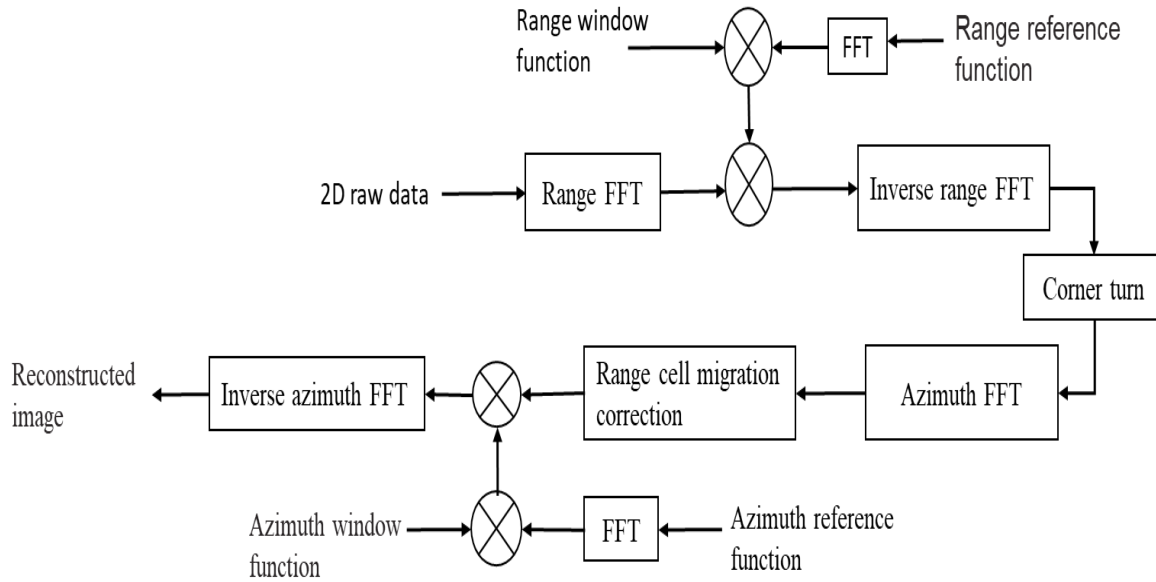
Figure 4.1. Range Doppler processing flow diagram**.**

First by applying the range Fourier transform on the 2D complex data using the range FFT block, followed by Fourier transforming the range reference function using the FFT block and multiplying with each row of the Fourier transformed 2D complex data and lastly the is inversely Fourier Transformed using the range IFFT block. The 'corner turn' transpose the range 2D range compressed complex data from row data to column data for subsequent azimuth compression. The transposed 2D complex data is Fourier transformed to Range-Doppler domain using the azimuth FFT block. If range cell migration correction is required, then it is applied at this stage. To compress the data in azimuth, first the azimuth reference function is Fourier transformed using the FFT block and multiplied with each row of the 2D complex data in range Doppler domain and lastly followed by taking inverse azimuth FFT of the product. After azimuth compression, the resulting image is the constructed image of targets that were focused. The study the Range-Doppler processing [29] algorithm is as follows.

38

4.1.1. Data Range Compression

The 2D data array of M rows and N columns can be seen in figure 4.2. Each row consists of N number digitalized data that serves as a single channel of range data for processing.

(a) M X N radar imaging data array

(b) Single channel radar range data
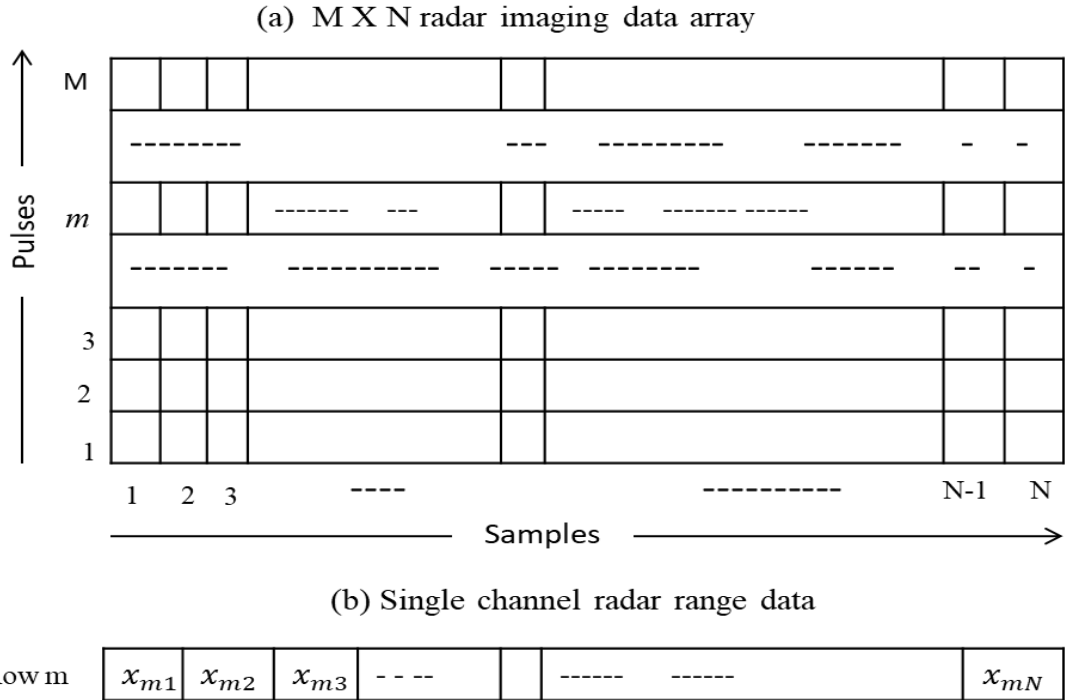
Figure 4.2. (a) M rows and N columns and (b) 1 row and N columns of the data arrays

The range compression of the raw data is performed by applying matched filter function on every row of range samples. From section 2.2.3, the matched filter function is designed as $h(t) = S^*(t)$ and its Fourier transform expressed as $H(f) = S^*(f)$, where $S^*(t)$ is the conjugate of transmitted signal. The matched filter function $h(t)$ is applied in the frequency domain by using the FFT on each row of the 2D complex data at a time during range compression process. A window function (padding) is applied on the matched filter to reduce the side lobe effects. After applying the matched filter function on each and every row data, the range IFFT is applied to the 2D range compressed data to transform to time domain.

4.1.2. Corner Turn

Figure 4.3. shows the operation of corner turn where the nth column of M x 1 data array is transposed or rotated horizontally as a row of 1 x M data array.
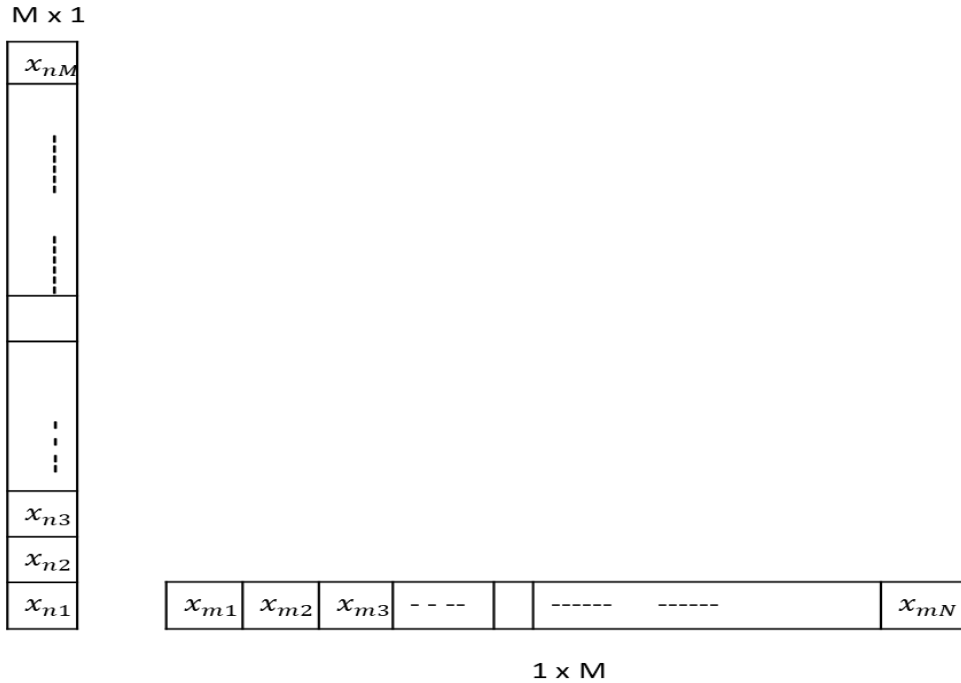
Figure 4.3. Corner turn operation

When processing a signal in range, the 2D data array are processed on a row basis retaining the same output. The edge effect of the circular [16] convolution is reduced by padding the row data and selecting the appropriate size of FFT. The corn-turn transpose the column data to row data azimuth FFT operation.

4.1.3. Range Cell Migration Correction (RCMC).

The RCMC is applied either in time or in range domain on the 2D range compressed complex data. The range migration amount is corrected in either range Doppler frequency domain. In range Doppler frequency or range partial (slow time). Multiples of equal targets slant ranges and their corresponding trajectories in range Doppler frequency domain appear as one while in range spatial domain, appear scattered along the azimuth [13].

40

4.1.3.1.   Range Migration Amount computation.

If r_{gr} is the closest ground range between the radar and the target and R_0 the shortest radar to target slant distance, then the slant range difference ΔR_s is obtained as:

$$\Delta R_s = R_0 - r_{gr} \ , \qquad R_0 > r_{gr} \tag{4.1}$$

Suppose the angle between the range axis and the slant range is ϕ , then

$$\Delta R_s = \frac{r_{gr}}{cos\phi} - r_{gr}$$

This equation gives the amount of the range migration needed for correction. The RCMC will be with respect to ground range r_{gr}.

Considering the Doppler frequency equation,

$$f_{dp} = \frac{2V}{\lambda} sin\phi,$$

The slant range difference ΔR_s can be expressed in terms of Doppler frequency as:

$$\Delta R_s = r_{gr} \left(1 - \left(\frac{f_{dp}\lambda}{2V} \right)^2 \right)^{-(1/2)} - r_{gr} \tag{4.2}$$

Suppose the total sample length of FFT is N, then the kth bin of Doppler frequency f_{dpk}, is

$$f_{dpk} = k \left(\frac{f_{PRF}}{N} \right),$$

Where f_{PRF} is the frequency along the azimuth direction (pulse repetition frequency).

So 4.2 becomes,

$$\Delta R_{sk} = r_{gr} \left(1 - \left(\frac{kf_{PRF}\lambda}{2NV} \right)^2 \right)^{-(1/2)} - r_{gr}$$

For high frequency Linear FM signals, $kf_{PRF}\lambda \ll 2NV$;

so,

41

$$\Delta R_{\text{sk}} \approx k^2 f_{PRF}^2 \lambda^2 r \Big/ 8N^2 V^2$$

Therefore, the number of range cells needed for a correction is,

$$\Delta N_{R_{\text{sk}}} = 2\Delta R_{\text{sk}} \Big/ R_s \approx k^2 f_{PRF}^2 \lambda^2 r \Big/ 4N^2 V^2 R_s \tag{4.3}$$

Where k = 1, 2, 3, ..., N, is with respect to target dependent ground range distance r_{gr}. Equation 4.3 works for broadside SAR systems well since the Doppler frequency is zero for broadside SAR systems whereas, in squint SAR system, equation 4.3 need to be modified in order for RCMC to depend on the shortest slant distance R, which corresponding to the Doppler frequency f_{dpL}.

$$\Delta R_s = R_0 - R = \frac{r_{gr}}{cos\phi} - \frac{r_{gr}}{cos(\varphi - 0.5 B_a)}$$

And

$$\Delta N_{R_s k} = 2\Delta R_{\text{sk}} \Big/ R_S \approx = \frac{\lambda^2 r_{gr} r}{4V^2 R_s}\left(f_{dpL} + \frac{k f_{PRF}}{N}\right)^2 - \frac{\lambda^2 r_{gr} f_{dpL}^2}{4V^2 R_s} \tag{4.4}$$

After the correction of range migration, range references will be corrected and by aligning either along the slant range R_s or along the reference range r_{gr}. For broadside SAR, the RCMC converts the slant range R_s to the range r_{gr}.

Since echo receiving time varies as the radar illuminates the targets within the time of the synthetic aperture length L_s, the sampling of the peaks of the range compressed signal may not occur correctly through the A/D converter having sampling frequency f_s. Therefore, to accurately correct the range cell migration, two major steps such as range sample shift and interpolation of fractional range sample are employed. However, the two steps can be performed in a single process. But for purpose of study, the two steps will be explained separately. Figure 4.4. illustrate the 2D data before RCMC. The data of the compressed pulse in the Doppler frequency do not aligned in azimuth but rather spread in range direction with varying magnitude of pulse peaks. This variation in magnitude result from inaccurate sampling of peak values at the peak points. To correct this, the range

migration amount is computed on all row data in the Doppler frequency bin then interpolating the digitalized samples by the range migration amount fractional part. The row data are the shifted with respect to a reference sample by range migration amount integer part.
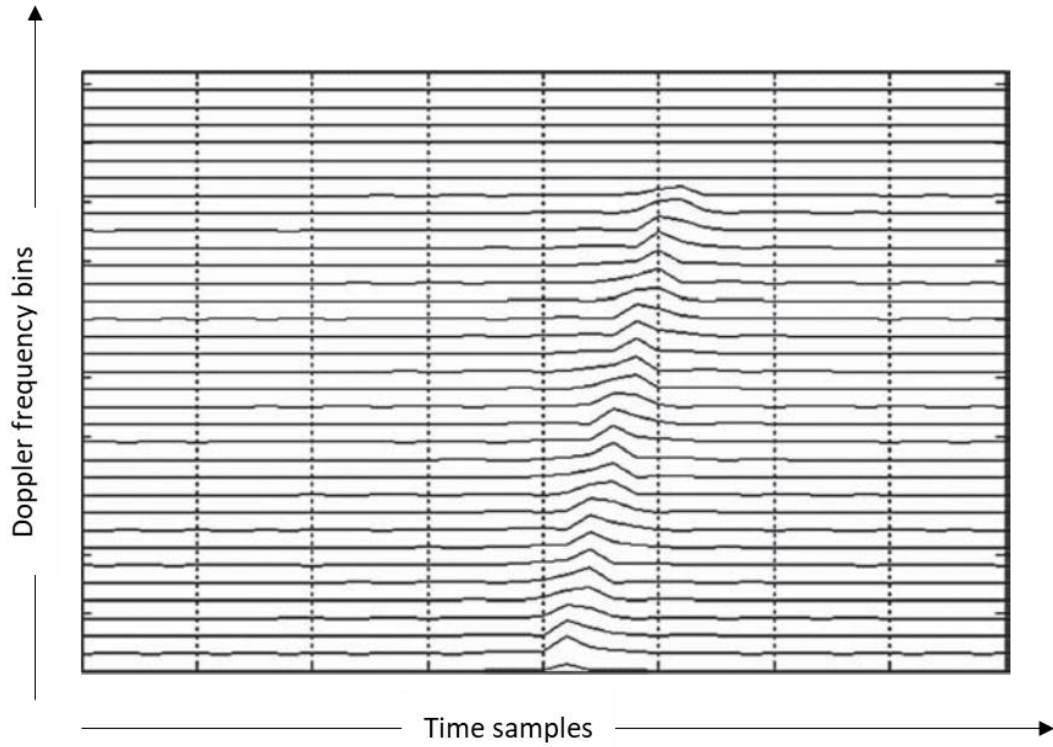
Figure 4.4. An illustration of Range compressed data without correction

4.1.3.2.   Interpolation by the fractional range sample.

The digitalized row samples of the signal are interpolated of by the fractional part of $\Delta N_{R_s k}$ in equation 4.4. First it starts by quantization of each computational fractional sample, chosen an appropriate sinc filter, convolving it with the entire row data resulting to interpolated signal with peak values properly positioned The interpolation is applied to all the row data along the Doppler frequency axis.

4.1.3.3. The Range Sample Shift.

Peak values that were not properly aligned are shifted left to align properly with the reference sample $N_r = f_s \tau_p$ by the integer part of range sample migration amount. The integer part of the range sample migration amount $\Delta N_{R_0 k}$ in 4.4 to align with the reference. The pulsed sampled array after sample shift is illustrated on figure 4.5.
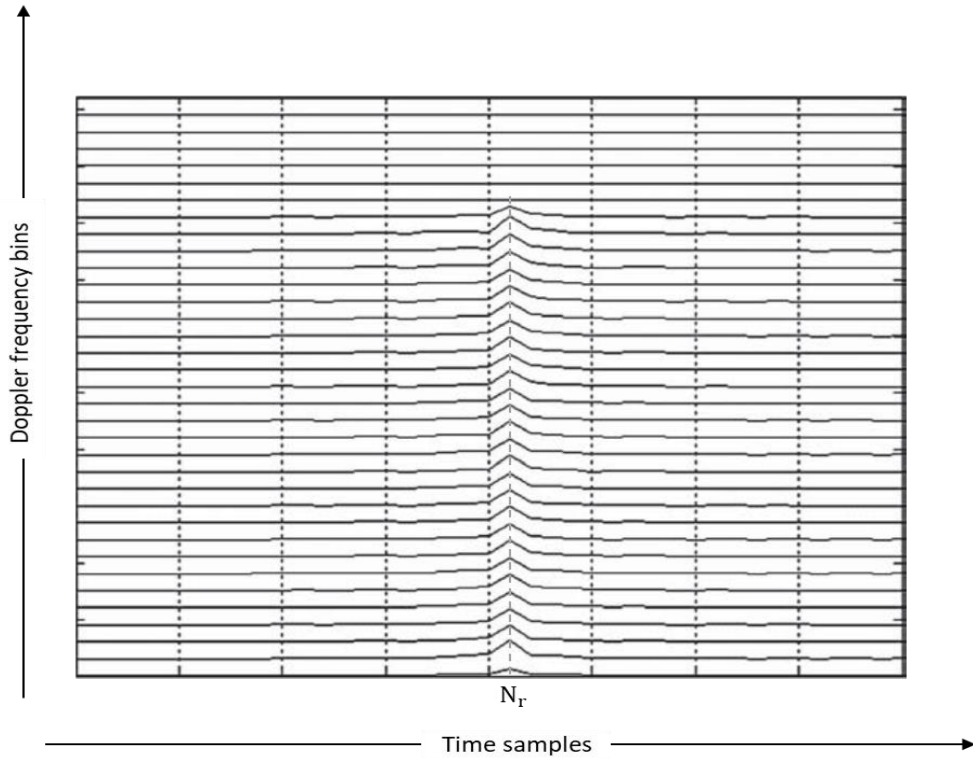
Figure 4.5. Compressed data array after sample shift

4.1.4. Azimuth Compression.

After the migrated cells are correction, a reference function, is applied to further compress the 2D data along the azimuth. The LFM waveform along the azimuth direction, which is similar to the ordinary LFM signal, serves as the azimuth matched filter for the azimuth compression. The LFM waveform in azimuth is specified by pulse duration time t_a, azimuth chirp rate (Doppler frequency changing rate) k_a and Doppler frequency centroid f_{dpc}.

4.1.4.1.   Doppler Frequency Centroid.

For a broadside SAR system, [13] Doppler Frequency Centroid f_{dpc} is equal to zero [9] while for squint SAR system is nonzero and is given as:

$$f_{dpc} = \frac{2V}{\lambda} \sin\varphi \tag{4.5}$$

Where φ is the squint angle , V velocity parameter and λ is the wavelength.

4.1.4.2.   Azimuth chirp Rate

The azimuth chirp rate (Doppler frequency change rate) k_a is obtained as:

$$k_a = \dot{f}_{dp} = -\frac{2V^2}{\lambda R_0} \cos^2\varphi_u.$$

Since only small squint angle and small radar beam width are always considered. For very small squint angle value, $\cos^2\varphi_u \approx 1$

Therefore k_a can be approximated as,

$$k_a \approx -\frac{2V^2}{\lambda R_0} \tag{4.6}$$

4.1.4.3.   Pulse Duration

The pulse duration t_a of the received signal in azimuth direction is obtained as follows

$$t_a = {L_s}/{V}, \tag{4.7}$$

Where L_s is synthetic aperture length and V is the radar velocity of the radar . For broadside and squint SAR systems, L_s is computed as follows;

For a broadside SAR system,

$$L_s = 2R_0 \tan(0.5B_a) \tag{4.8}$$

Squint SAR with squint angle φ:

$$L_s = R_0 \tan(\varphi + 0.5B_a) - R_0 \tan(\varphi - 0.5B_a) \tag{4.9}$$

45

Where B_a is the radar bandwidth. Since R_0 depends on synthetic aperture length L_s and target location therefore, the pulse duration t_a depends on range. Thus, the azimuth reference also depends on range, and therefore, azimuth compression is performed with a different azimuth reference function.

4.1.5. Reconstruction of Radar Image using Range-Doppler processing.

A satellite-based (ERS) raw data generated by ESA, processed and distributed by German Aerospace Center, DLR will be used in reconstructing the radar image using Range Doppler algorithm. The parameters ERS SAR sensor parameters are listed [3] on table 4.

The chirp signal of the radar is represented [3] as:

$$s(\tau) = exp(j\pi k_r \tau^2), \tag{4.10}$$

Where the chirp length $\tau = -\tau_p \leq \frac{1}{f_s} \leq \tau_p$ with $\tau_p = 3.712 \ x \ 10^{-5} s$, the range Sampling frequency $f_s = 18.962468 \ x \ 10^6$ and chirp rate $k_r = 4.18989015 \ x \ 10^{11} s^{-2}$

Table 4. ERS sensor parameters

	Parameters		Value	Unit
Parameters for range compression	Range sampling frequency	f_s	18.962468 x10^6	s^{-1}
	Chirp rate	k_r	4.18989015x10^{11}	s^{-2}
	Chirp length	τ_p	37.12x10^{-6}	s
Parameters for azimuth compression	Velocity parameter	V	7098.0194	m/s
	Wavelength	λ	0.05656	m
	Range to target at broadside time t = 0	R_0	852358.15	m
	Aperture time	t_a	0.6	s
	Pulse repetition frequency	PRF	1679.902	s^{-1}

Figure 4.6. displays the waveform of chirp signal of equation 4.10.
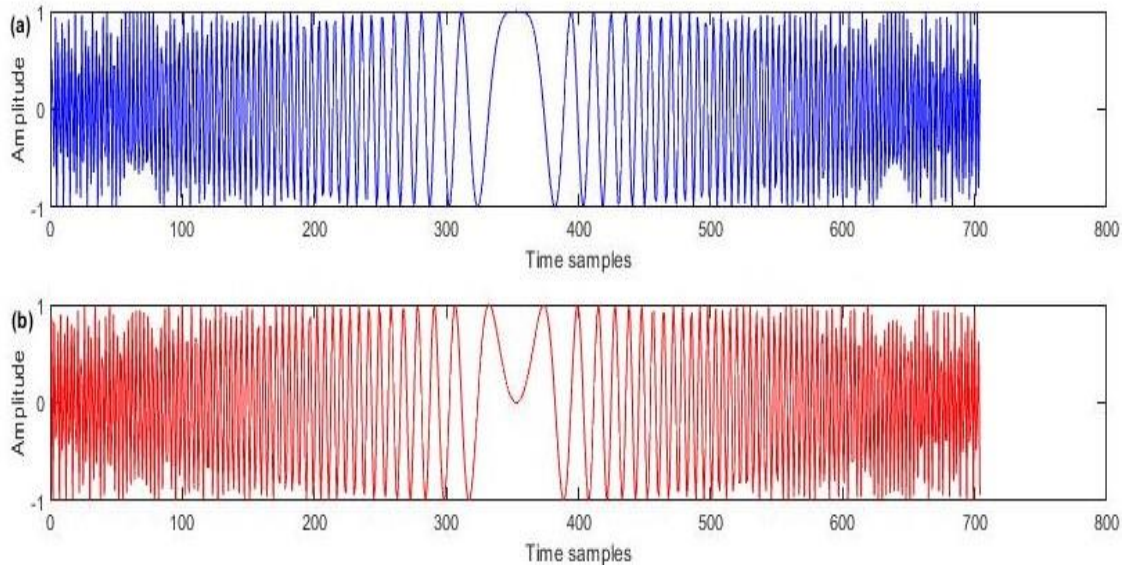
Figure 4.6. Chirp signal waveforms. (a) real and (b) imaginary parts of the signal.

Figure 4.6 represent the waveforms of the chirp signal array of equation 4.10. The time samples of sampling rate 19MHz are presented by the horizontal axis. The number of samples within a LFM pulse (each azimuth line), $f_s \tau_P = 704$. The number of azimuth lines are represented by the vertical axis.
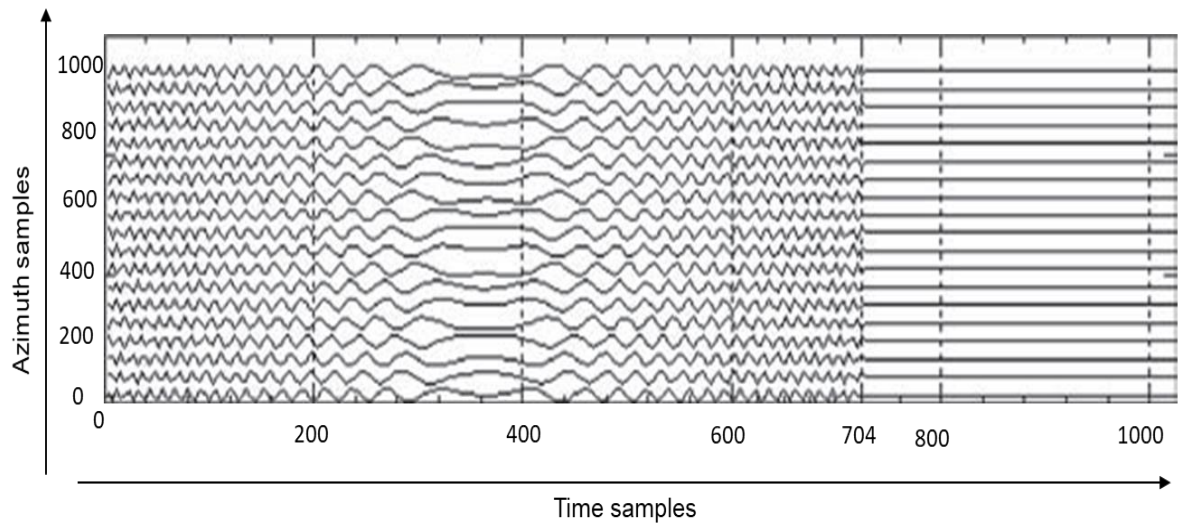
Figure 4.7. Waveforms of chirp signal array of equation 4.10

The range reference function is expressed [8] as:

$$h_{rf}(\tau) = s^*(\tau) = exp(-j\pi k_r \tau^2)$$

Figure 4.8. displays the real part and the imaginary part of the range matched filter $h_{rf}(\tau)$.
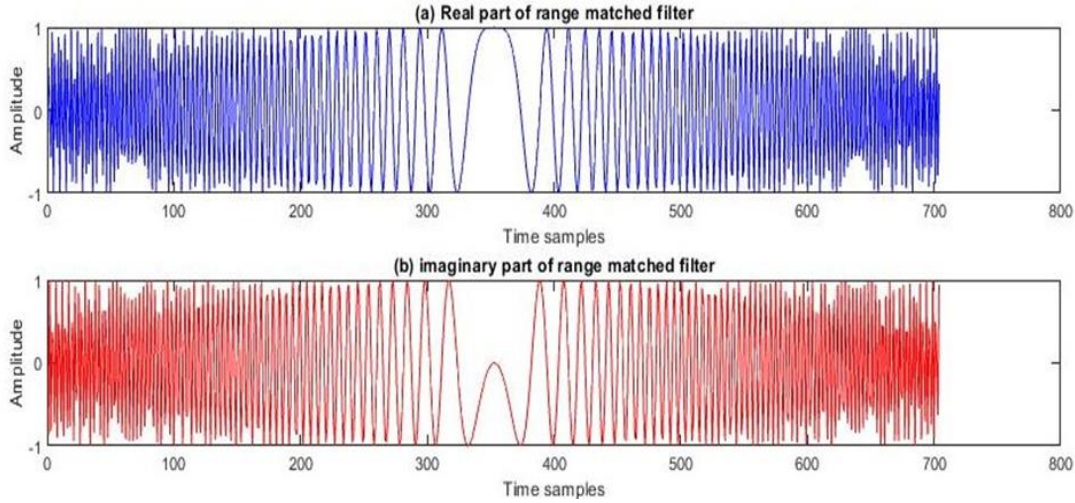
Figure 4.8. Range reference function

The sampling frequency is 18.962468 $\times 10^6 s^{-2}$ for range (or time) signal. In the range reference function $h_{rf}(\tau)$, there will be a total of 704 samples corresponding to the sample number of pulse duration 3.712 x 10^{-5}s. The real parts of the chirp signal $S(\tau)$ and the range reference function $h_{rf}(\tau)$ are identical whereas the imaginary part of the chirp signal $S(\tau)$. of is negative that of the range reference function $h_{rf}(\tau)$.

The azimuth matched filter [8] is designed as:

$$h_{af}(t) = S^*(t) = exp(-j\pi k_a t^2)$$

Where the time length in azimuth $t = -\frac{t_a}{2} \leq \frac{1}{PRF} \leq \frac{t_a}{2}$, with aperture time $t_a = 0.6s$ and the parameter frequency modulation rate in azimuth k_a can be obtained as follows:

$$k_a = -\frac{2V^2}{\lambda R_0}$$

With the velocity parameter $V = 7098.0194 ms^{-1}$, $R_0 = 852358.15m$ and $\lambda = 0.05656m$

Therefore,

$$k_a = -2090.13s^{-2}$$

Figure 4.9 displays the azimuth reference function with sampling frequency $1679.02s^{-1}$ for the azimuth signal. The total number of samples of the azimuth reference function is:

$$N_{az} = {L_s}/{A_s} = 1008$$

Where the azimuth sample spacing $A_s = {V}/{PRF} = 4.23m$, azimuth pulse $t_a = {L_s}/{V} = 0.6s$. and L_s is the synthetic aperture length.
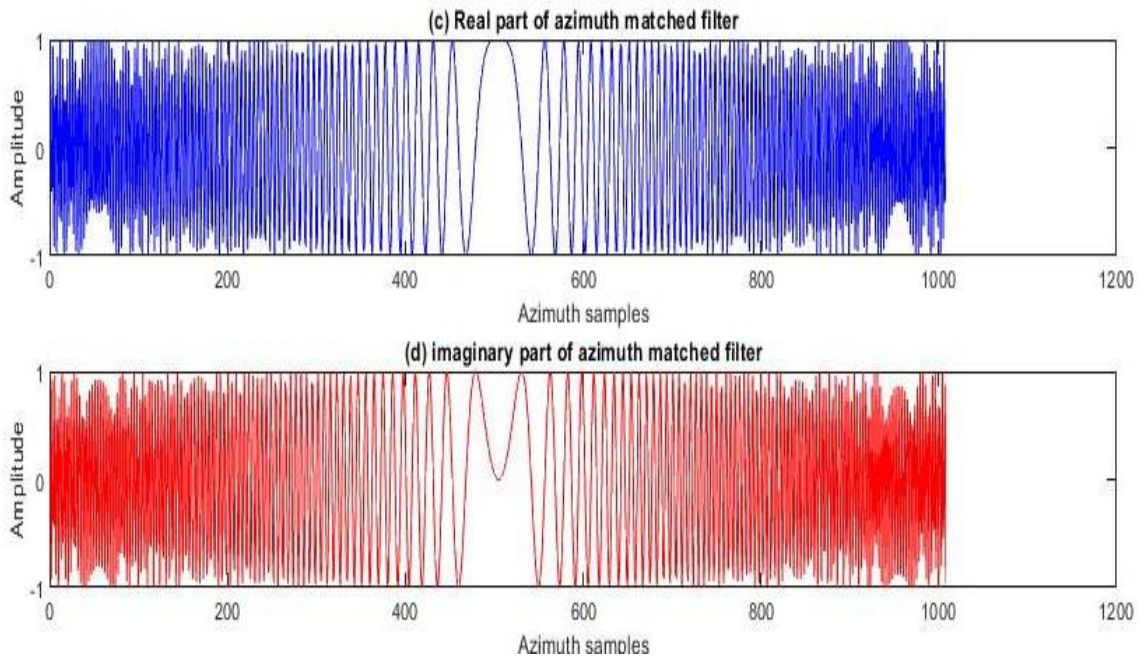
Figure 4.9. c) The real part and d) the imaginary part of Azimuth matched filter.

Figure 4.10. displays the spectra of range and azimuth matched filters

49
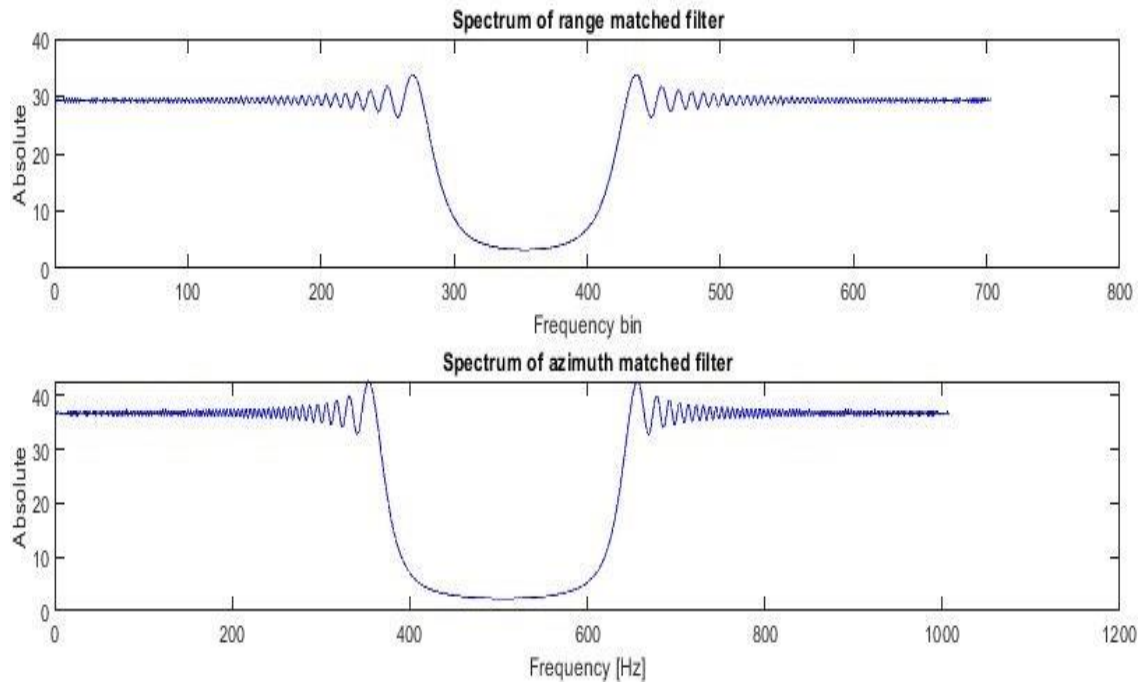
Figure 4.10. spectra of range and azimuth matched filters

The ERS raw data is shown in Figure 4.11.
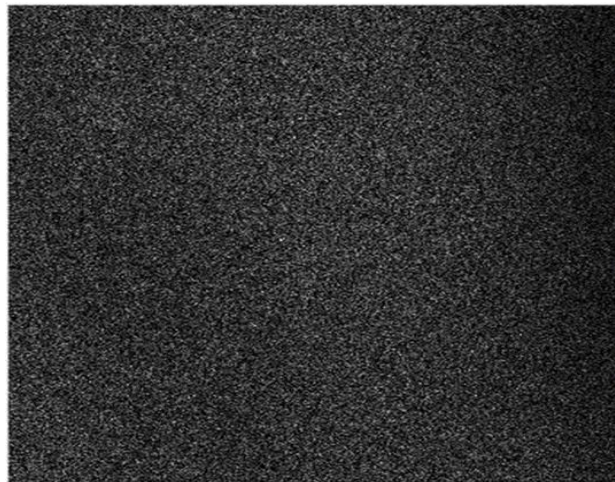
Figure 4.11 ERS data

The operation of range compression is performed by first transforming each row of the data into the frequency domain by applying range FFT. Since there is 704-time sample for each azimuth line, zero paddings are required for the range compression. The Fourier

transformed match filter is then multiplied with every row of the frequency domain data. The range compressed data in frequency domain result is transformed back to time domain using range inverse FFT. Figure 4.12 shows the range compressed data. After range compression, the next operation to [16] perform is the azimuth compression. In azimuth compression, each column of the range compressed data and the azimuth matched filter are transformed in to Doppler frequency domain by azimuth FFT. Since The reference function $H_{af}(f)$ in Doppler frequency domain has the total number of 1008 samples, zero paddings are required to increase the azimuth samples number to the total length of 2048 (length of the data).
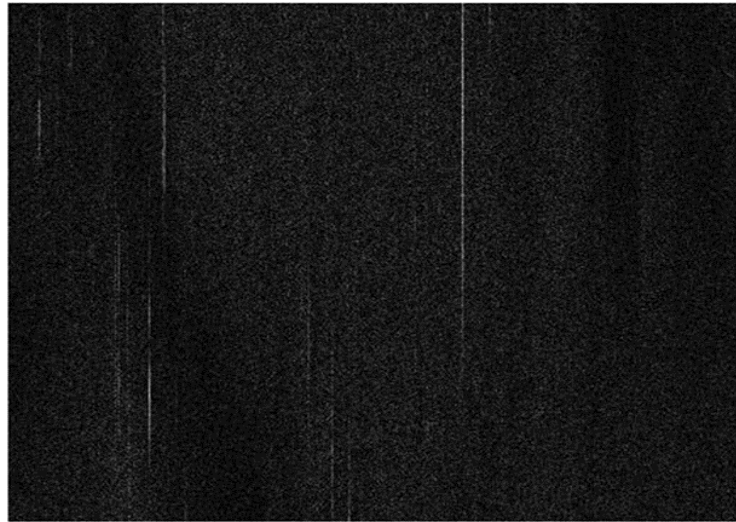
Figure 4.12 Range-compressed signal

The azimuth reference function $H_{af}(f)$ is multiplied with each column of the range-Doppler frequency domain data and the product is inversely Fourier transformed using azimuth inverse FFT to get the processed image as shown on Figure 4.13.
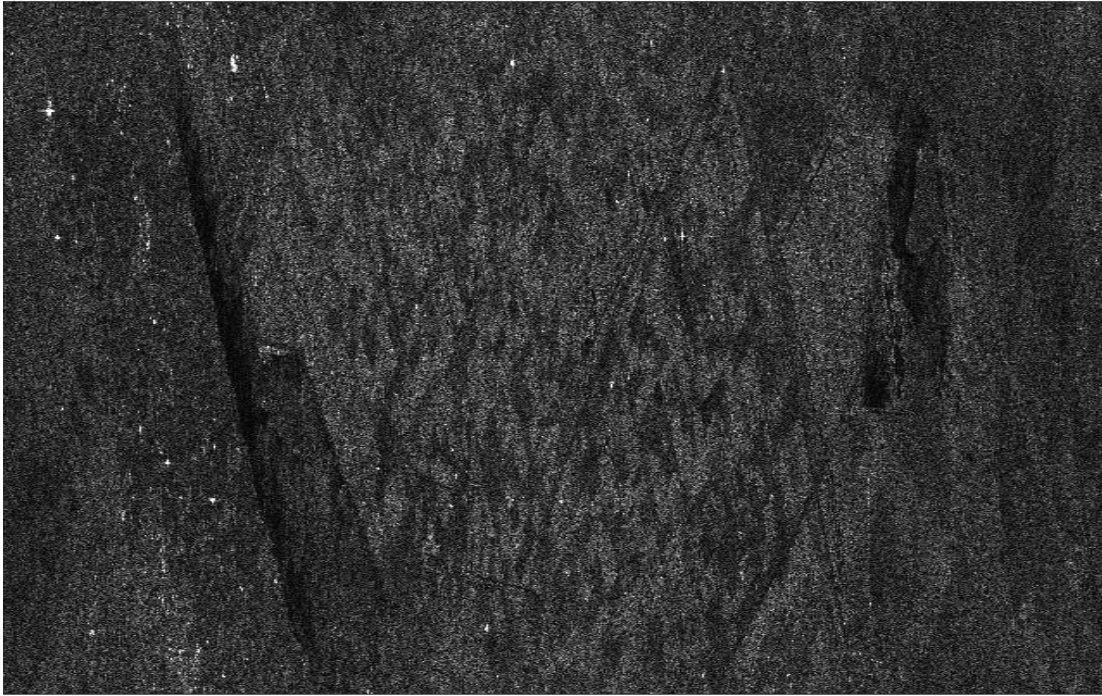
Figure 4.13. Constructed Image

The processed image or single look complex image, is highly speckled as seen in figure 4.13. To reduce the effect speckle on the processed data, the image processing technique such as multi-look and spatial processing will be applied to the image. The single look complex image depends on the range and azimuth pixels. The range pixel depends on sampling frequency, look angle and radar wave speed, while the azimuth pixel depends on the radar speed and the pulse repetition frequency. To increase the resolution of the single look complex image, multi-look processing is applied to enable pixels to have the same size in azimuth and range direction [12]. In the single look complex data, the pixel size is approximately 25m x 5m. Figure 4.14 displays the multilook image of figure 4.13, where average 5 azimuth pixels to one azimuth pixel.
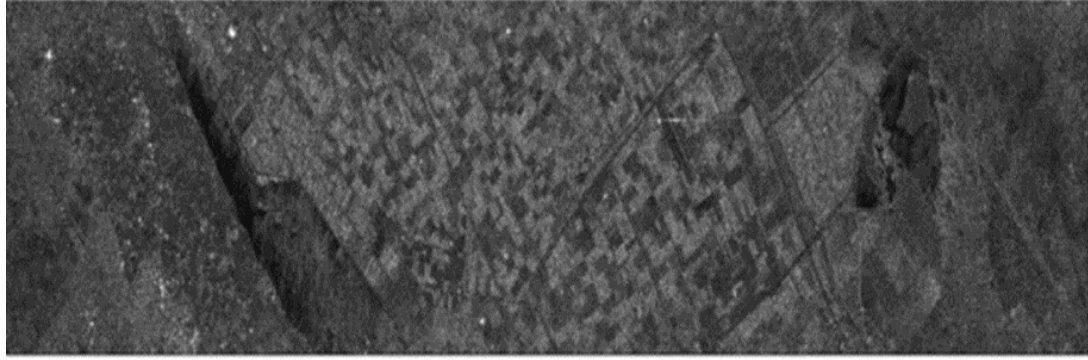
Figure 4.14 Image after multilook and spatial processing

The image after multilook processing is made of amplitude values rather than complex values for the single look image. Speckle reduction can also be achieved by applying Single-channel filters such as the Lee and Frost filter to the SAR processed image.

4.2. Stolt interpolation processing of SAR data

4.2.1. Stolt interpolation System model.

Figure 4.15. displays a system configuration for 3D radar signal processing. In this configuration, the radar is considered to be located at (0, 0, h) and moving at the speed V along the flight path [13].

The SAR emits a pulse at time $t = 0$ and received the echo after a short delay. Assuming that the targets with the shortest slant range R_S and the longest slant range R_L are distributed along the x-axis, then,

The echo delay time at the distances R_s is:

$$t_0 = {2R_s}/{c} = {2x_0}/{c\sin\theta}$$
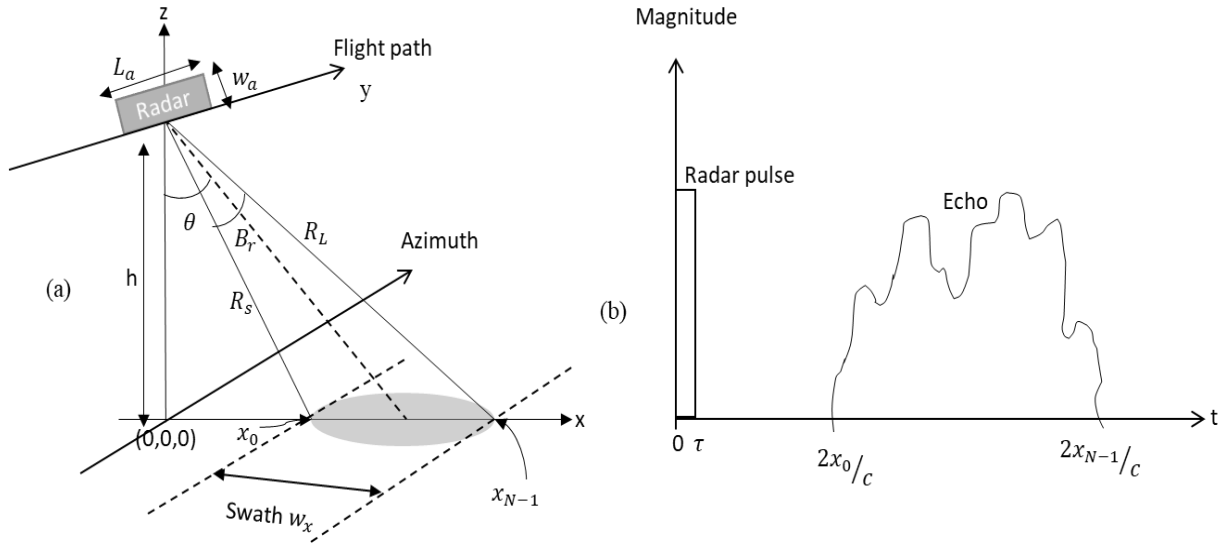
Figure 4.15 (a) Imaging radar and (b) the radar pulse and echo

The echo delay time at the distance R_L is:

$$t_{N-1} = \frac{2R_L}{c} = \frac{2x_{N-1}}{c\sin\theta}$$

The corresponding ground ranges at t_0 and t_{N-1} are: $x_0 = \frac{c}{2}(t_0\sin\theta)$ and $x_{N-1} = \frac{c}{2}(t_{N-1}\sin\theta)$ respectively. The swath width w_x starts at x_0 and ends at x_{N-1}. The swath width w_x and the radar band width B_r are related as:

$$w_x \approx \frac{B_r}{2}(R_s + R_L) = \frac{\lambda}{2w_a}(R_s + R_L)$$

Where $B_r = \frac{\lambda}{w_a}$, w_a is the radar antenna width and λ the wavelength of radar wave.

The relationship between echoes and the pulse of the radar is shown figure 4.15(b), where the echo return time is indicated by the horizontal axis. The parameters x and t can be used interchangeably since they are related by:

$$t = 2\left(\frac{x}{c}\right)$$

Figure 4.16. shows an ideal target function $g_\sigma(x)$ with N discrete point targets located at x_n. The magnitude of each target is denoted by the reflective coefficient σ_n ,

54

where $n = 0, 1, 2, 3, . . ., N$. The reflective coefficients σ_i appears on radar image as bright or dark dots
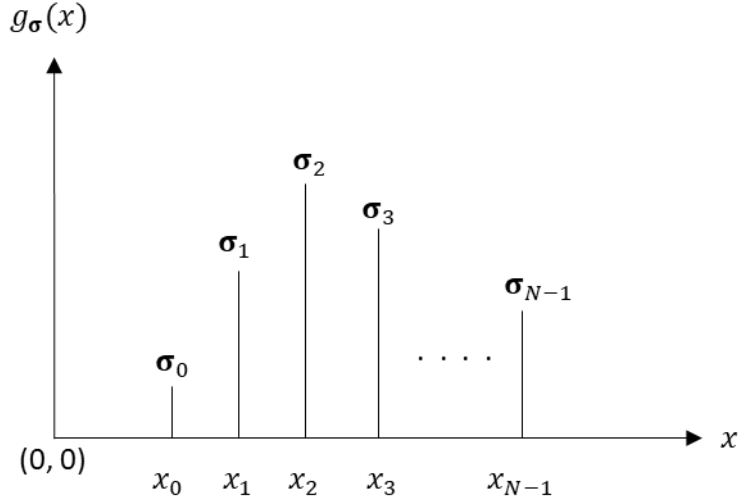
Figure 4.16. An ideal target function.

The targets locations are identified by the function along $g_\sigma(x)$ as;

$$g_\sigma(x) = \sum_{n=0}^{N-1} \sigma_n \delta(x - x_n) \tag{4.11}$$

Suppose, N targets are distributed randomly with each located at the point (x_n, y_n), where $n = 1, 2, 3, ..., N$. If the radar is at the point $(0, u)$, transmitting pulses $p_\sigma(t)$ on two-dimensional target area in range x, then the total received [9] signal $S_\sigma(t, u)$ becomes

$$S_\sigma(t, u) = \sum_n \sigma_n\, p_\sigma\left(t - \frac{2\sqrt{x_n^2 + (y_n - u)^2}}{c}\right) \tag{4.12}$$

Where the function $S_\sigma(t, u)$, depends on time t, and radar position u. Applying 2D Fourier transform on the function with respect to the time variable $t_n = \dfrac{2\sqrt{x_n^2 + (y_n - u)^2}}{c}$ becomes

$$S_\sigma(\omega, u) = \sum_n \sigma_n\, P_\sigma(\omega) exp\left\{-j\frac{2\omega}{c}\sqrt{x_n^2 + (y_n - u)^2}\right\}$$

Where $P_\sigma(\omega)$ is the Fourier transform of $p_\sigma(t)$.

The signal $S_\sigma(\omega, u)$ is partial Fourier transform with respect to u (spatial variable) as

$$S_\sigma(\omega, \omega_{dp}) = P_\sigma(\omega) \sum_n \sigma_n \, exp\left\{-j\sqrt{4\left(\frac{\omega^2}{c^2}\right) - \frac{\omega_{dp}^2}{V^2}}\, x_n - j\left(\frac{\omega_a}{V}\right)y_n\right\} \tag{4.13}$$

Where $\frac{\omega_{dp}}{V}$ is the partial waveform number in Doppler frequency domain, with ω_{dp} the Doppler angular frequency.

Suppose the reference target location $(x_n, y_n) = (x_c, 0)$, where x_C is the distance of the radar (at any synthetic aperture position u) from the center of the swath, then,

$$S_{\sigma 0}(\omega, \omega_{dp}) = P_\sigma(\omega) \sum_n \sigma_n \, exp\left\{-j\sqrt{4\left(\frac{\omega^2}{c^2}\right) - \left(\frac{\omega_{dp}^2}{V^2}\right)}\, x_c\right\}$$

Assuming the targets are ideal with reflection coefficients $\sigma_n = 1$, for n = 1, 2,. . . , N. Therefore,

$$S_{0\sigma}(\omega, \omega_{dp}) = P_\sigma(\omega) exp\left\{-j\sqrt{4\left(\frac{\omega^2}{c^2}\right) - \left(\frac{\omega_{dp}^2}{V^2}\right)}\, x_c\right\} \tag{4.14}$$

And,

$$S_{0\sigma}^*(\omega, \omega_a) = P_\sigma^*(\omega) exp\left\{j\sqrt{4\left(\frac{\omega^2}{c^2}\right) - \left(\frac{\omega_{dp}^2}{V^2}\right)}\, x_c\right\} \tag{4.15}$$

The function $S_{0\sigma}^*(\omega, \omega_a)$ is a 2D matched filter on both ω and ω_{dp} domain [18], [13].

- $P_\sigma^*(\omega)$ is the range matched filter

- $exp\left\{\left[j\sqrt{4\left(\frac{\omega^2}{c^2}\right) - \left(\frac{\omega_{dp}^2}{V^2}\right)}\right]x_c\right\}$ is considered as 2D azimuth reference function

Therefore, the 2D compression of the $S_\sigma(\omega, \omega_{dp})$ is expressed as

$$S_{\sigma c}(\omega, \omega_{dp}) = S_\sigma(\omega, \omega_{dp})S_{0\sigma}^*(\omega, \omega_{dp})$$

$$= P_\sigma(\omega)P_\sigma^*(\omega) \sum_n exp\left\{-j\left[\sqrt{4\left(\frac{\omega^2}{c^2}\right) - \left(\frac{\omega_{dp}^2}{V^2}\right)}\right](x_n - x_c) - j\left(\frac{\omega_{dp}}{V}\right)y_n\right\}$$

56

If the partial waveform number $\frac{\omega_{dp}}{V} = k_y = k_u$, and $\frac{\omega}{c} = k$, then the 2D compressed signal $S_{\sigma c}(k, k_u)$ can [18], [13] be obtained as:

$$S_{\sigma c}(k, k_u) = |P_\sigma(k)|^2 \sum_n exp\left\{-j\sqrt{4k^2 - k_u^2}(x_n - x_c) - j(k_u)y_n\right\}$$

Or,

$$S_{\sigma c}(k_x, k_y) = |P_\sigma(k)|^2 \sum_n exp\left\{-jk_x(x_n - x_c) - j(k_y)y_n\right\} \tag{4.16}$$

Where $k_x = \sqrt{4k^2 - k_u^2}$.

Only targets located at the point $(x, 0)$ will be correctly focused since the 2D azimuth matched filter was chosen correctly [13] at the point $(x_c, 0)$. Other targets located away from this will be unfocused. The unfocused targets will require more accurate correction or compression method. Suppose the carrier frequency f_c, bandwidth frequency f_b and bandwidth $2f_0$ of the transmitting signal [18], satisfies the relationship; $\omega_c - \omega_0 \le \omega \le \omega_c + \omega_0$, where $\omega = \omega_c + \omega_b$, in terms of [18] wavenumber the relation can be represented as $k_c - k_0 \le k \le k_c + k_0$, with $k = k_c + k_b$. Since $k_c \gg k_b$, therefore $k \cong k_c$.

The phase [18] function $\sqrt{4k^2 - k_u^2}(x_n - X_c)$ from equation 4.16 can be expressed as follows

$$\sqrt{4k^2 - k_u^2}(x_n - X_c) = 2k\left(1 - \frac{k_u^2}{4k^2}\right)^{1/2}\Delta x_n = 2k_c\left(\frac{4(k_c + k_b)^2 - k_u^2}{4k_c^2}\right)^{1/2}\Delta x_n$$

$$\sqrt{4k^2 - k_u^2}(x_n - X_c) = 2k_c\left(1 - \frac{k_u^2}{4k_c^2} + \frac{2k_b}{k_c} + \frac{k_b^2}{k_c^2}\right)^{1/2}\Delta x_n$$

Let $\gamma^2 = 1 - \frac{k_u^2}{4k_c^2}$, then ,

$$\sqrt{4k^2 - k_u^2}(x_n - X_c) = 2k_c\left(\gamma^2 + \frac{2k_b}{k_c} + \frac{k_b^2}{k_c^2}\right)^{1/2}\Delta x_n$$

57

$$= 2k_c \left(\gamma + \frac{k_b}{\gamma k_c} + \frac{k_b^2}{2\gamma k_c^2} + \ldots \right) \Delta x_n \qquad (4.17)$$

Since $k_c \gg k_b$ and $k_c \gg k_u$, then 4.17 can approximated as:

$$\sqrt{4k^2 - k_u^2}(x_n - X_c) \approx 2k_c \left(\gamma + \frac{k_b}{\gamma k_c} \right) \Delta x_n = 2\left(\gamma k_c + \frac{k_b}{\gamma} \right) \Delta x_n \qquad (4.18)$$

Substituting 4.17 into 4.16, gives,

$$S_{\sigma c}(k, k_u) = |P_\sigma(k)|^2 \sum_n exp\left\{ -j2\left(\gamma k_c + \frac{k_b}{\gamma} \right) \Delta x_n - j(k_u)y_n \right\} \qquad (4.19)$$

From equation 4-16, $k_x = \sqrt{4k^2 - k_u^2}$, relating with equation 4.18, then

$$k_x = 2\left(\gamma k_c + \frac{k_b}{\gamma} \right)$$

Let $k_x = k_c + k_{xb}$, where k_{xb} is the baseband signal of k_x then,

$$k_c + k_{xb} = 2\left(\gamma k_c + \frac{k_b}{\gamma} \right)$$

$$k_{xb} = (2\gamma - 1)k_c + \frac{2k_b}{\gamma}$$

From $\gamma = \left(1 - \frac{k_y^2}{4k_c^2} \right)^{1/2}$ implies $\gamma \approx 1 - \frac{k_y^2}{8k_c^2}$ and also $\frac{1}{\gamma} \approx 1 + \frac{k_y^2}{8k_c^2}$

Therefore,

$$k_{xb} = (2\gamma - 1)k_c + \frac{2k_b}{\gamma} = k_c - \frac{k_y^2}{4k_c} + 2\left(1 + \frac{k_y^2}{8k_c^2} \right)k_b \qquad (4.20)$$

Equation 4.20 shows the transformation in the baseband situation of k to k_x.

Assuming $|P_\sigma(k)| = 1$, then equation 4.15 can be expressed in [18], [13] the baseband situation as

$$S_{\sigma c}(k_b, k_y) = \sum_n exp\{ -jk_{xb}(x_n - X_c) - j(k_y)y_n \} \qquad (4.21)$$

Substituting 4.20 into 4.21, gives

$$S_{\sigma c}(k_b, k_y) = \sum_n exp\left[-j\left\{ k_c - \frac{k_y^2}{4k_c} + 2\left(1 + \frac{k_y^2}{8k_c^2} \right)k_b \right\} \Delta x_n - j(k_y)y_n \right]$$

58

$$S_{\sigma c}(k_b, k_y) = \sum_n exp\left[j\left\{-k_c + \frac{k_y^2}{4k_c} - 2\left(1 + \frac{k_y^2}{8k_c^2}\right)k_b\right\}\Delta x_n - j(k_y)y_n\right]$$

$$S_{\sigma c}(k_b, k_y) = \sum_n exp\left[j\left\{-\left(2 + \frac{k_y^2}{4k_c^2}\right)k_b + \frac{k_y^2}{4k_c} - k_c\right\}\Delta x_n - j(k_y)y_n\right] \quad (4.22)$$

$$\text{Let } k_{ab} = \left(2 + \frac{k_y^2}{4k_c^2}\right)k_b \text{ and } k_{a0} = \left(\frac{k_y^2}{4k_c} - k_c\right)$$

$$S_{\sigma c}(k_{ab}, k_y) = \sum_n exp\left[-j(k_{ab} - k_{a0})\Delta x_n - j(k_y)y_n\right]. \quad (4.23)$$

Suppose $s_\sigma(x)$ and $S_\sigma(k_\alpha)$, are a pair of Fourier Transform, then by the modulation and the shift property,

$$S_\sigma(k_\alpha - k_{a0}) <=> s_\sigma(x)exp(-jk_{a0}x)$$

From 4.23, the term k_{a0} shows that the compressed signal $S_{\sigma c}(k_b, k_y)$ in the wavenumber (k_{ab}) domain has a k_y-dependent shift of $k_{a0} = \left(\frac{k_y^2}{4k_c} - k_c\right)$. This means to correct the constant frequency shift, the corresponding spatial domain function in range-Doppler domain $S_{\sigma c}(x, k_y)$, should [13], [18] be multiplied by $exp\left\{-j\left(\frac{k_y^2}{4k_c} - k_c\right)\Delta x_n\right\}$. That is,

$$S'_{\sigma c}(x, k_y) = S_{\sigma c}(x, k_y)exp\left\{-j\left(\frac{k_y^2}{4k_c} - k_c\right)\Delta x_n\right\} \quad (4.24)$$

The value k_c in 4.24 is the constant wavenumber that corresponds to the carrier frequency of the radar signal. The value k_c will not affect the quality of the constructed radar image and therefore 4.24 can be written in a simplified form [9] as

$$S'_{\sigma c}(x, k_y) = S_{\sigma c}(x, k_y)exp\left\{-j\left(\frac{k_y^2}{4k_c}\right)\Delta x_n\right\} \quad (4.25)$$

Equation 4.25. is the differential azimuth compression since it performs spatial shifting of Δx_n on $S_{\sigma c}(x, k_y)$, and also provides a shift quantity $\left(\frac{k_y^2}{4k_c}\right)$ which depends on the azimuth value, k_y.

Figure 4.17 displays the diagram of SAR raw data processing by Stolt interpolation algorithm.
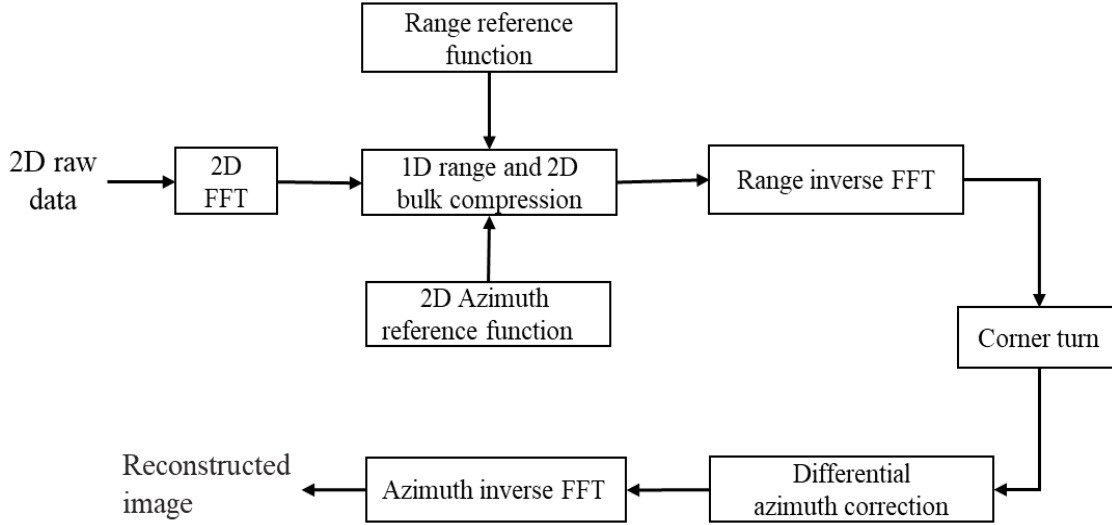
Figure 4.17. Block diagram of Stolt interpolation algorithm.

4.2.2. Reconstruction Algorithm for Stolt Interpolation Processing.

To compress the data in range, the signal array $S_\sigma(t, u)$ in 4.12 is 2D Fourier transformed to $S_\sigma(\omega, \omega_{dp})$ as shown in equation 4.13. The 2D Fourier Transformed signal $S_\sigma(\omega, \omega_{dp})$, will then be multiplied with the range matched filter $P_\sigma^*(\omega)$ to obtain a range compressed data $S_{\sigma c1}(\omega, \omega_{dp})$. The range compressed data array $S_{\sigma c1}(\omega, \omega_{dp})$ is then inverse-Fourier-transformed to range Doppler frequency domain signal $S_{\sigma c1}(t, \omega_{dp})$.

The next operation is the azimuth compressing which is done as follows.

1. By applying 1D azimuth matched filter in slow time t. With frequency changing rate k_a and the Doppler frequency f_{dp} (f_{dp}=0, for broadside case), the 1D reference function is obtained as follows:

$$h_{af}(t) = exp[-j\pi k_a(m\Delta t)^2],$$

where the frequency changing rate $k_a = \frac{-2V^2}{\lambda R_0}$, the pulse repetition interval $\Delta t = \frac{1}{f_{PRF}}$ and $-N_{azr} \leq m \leq N_{azr}$. The sample number N_{azr} corresponds to the reference

60

point located at R_0. The reference function $H_{af}(\omega_{Dp})$ is obtained by taking FFT on $h_{af}(t)$, with $t = m\Delta t$.

2. By applying the 2D azimuth matched filter. From 4.15 the 2D azimuth matched filter is gotten by discarding the range 1D reference function $P_\sigma^*(\omega)$.

$$H_{af}(\omega, \omega_{dp}) = exp\left\{j\left[\sqrt{4\left(\frac{\omega^2}{c^2}\right) - \left(\frac{\omega_{dp}^2}{V^2}\right)}\right]x_c\right\}$$

Where the frequency ω_{dp} corresponds to the true Doppler frequency and ω is the time domain signal passband frequency, that is $\omega_c - \omega_0 \leq \omega \leq \omega_c + \omega_0$, with ω_c as the carrier frequency, and $2\omega_0$ the bandwidth of the transmitting signal. The center of the target location x_C, of the radar (from the center of the swath) is invariant in the coordinates of the radar $(0, u)$ in stripmap SAR.

In broadside SAR, where no range migration correction is needed, the 2D azimuth matched filter $H_{af}(\omega, \omega_{dp})$ is approximated to 1D azimuth match filter $H_{af}(\omega_{dp})$ while in squint SAR case where range migration correction is require, both 1D and 2D filters are applied. The compression in azimuth is carried out by multiplying each column of the range compressed data $S_{\sigma c1}(t, \omega_{dp})$ with the azimuth matched $H_{af}(\omega_{dp})$ to obtain 2D compressed data $S_{\sigma c}(t, \omega_{dp})$. After the azimuth compression, the resulting 2D compressed signal $S_{\sigma c}(t, \omega_{dp})$ is a roughly compressed signal along azimuth direction, since the azimuth compression on the whole data is done by one filter. The Stolt interpolation will then be applied on the 2D azimuth compressed data $S_{\sigma c}(t, \omega_{dp})$ to improve the image quality through the differential azimuth compression based on 4.25.

$$S_{\sigma c}'(x, k_y) = S_{\sigma c}(x, k_y)exp\left[-j\left(\frac{k_y^2}{4k_c}\right)\Delta x_n\right]$$

The differential azimuth compression requires the computation of the following terms;

First the computation of range difference $\Delta x_n = (x_n - x_c)$ where x_c and x_n are the range values along the range axis. The range difference Δx_n can be calculated as

61

$$\Delta x_n = {}^{c}\!/_{f_s} (n - N_r),$$

where N_r corresponds to the range sample at x_c for $n = 1,2,3, \ldots, N_x$ along the range axis. Second the computation of the constant phase $k_y^2/4k_c$, where $k_c = {}^{\omega_c}\!/_{c}$ and the azimuth value $k_y = 2\pi m f_{PRF}/V N_y$, with m = 1, 2, 3, ..., N_y.

For any Doppler-frequency axis value m, the value of k_y is computed first then followed by the multiplication of every range sample $S_{\sigma c}(t, \omega_{dp})$ by $exp\left\{-j\left(\frac{k_y^2}{4k_c}\right)\Delta x_n\right\}$.

After differential azimuth compression, the azimuth inverse FFT with respect to ω_{dp} is applied, to obtained the constructed image.

4.2.3. Reconstruction of Radar Image Using Stolt Interpolation Algorithm.

In this section, a satellite-based (ERS) raw data generated by ESA, processed and distributed by German Aerospace Center, DLR will be used in reconstructing the radar image using Stolt Interpolation Algorithm. The parameters of the [8] sensor are listed on table 4.

The received data $S_{\sigma b}(m, n)$ with the number of azimuth lines, $m = 1, 2, 3, ..., 2048$ and the range samples $n = 1, 2, 3, ...,2048$, is compressed in range by applying the range reference function.
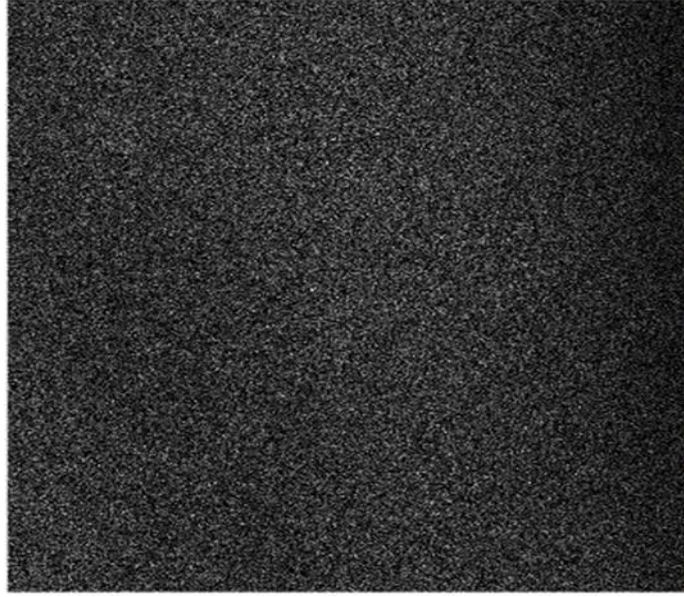
Figure 4.17. Raw data

The range reference function can be designed as:

$$h_{rf}(\tau) = exp[-j\pi k_r \tau^2]$$

Where the sampling interval $\tau = -\dfrac{\tau_p}{2} \leq \dfrac{1}{f_s} \leq \dfrac{\tau_p}{2}$, $k_r = 4.18989015 \times 10^{11} s^{-2}$, the sampling frequency $f_s = 18.962468 \times 10^6 s^{-1}$ and $\tau_p = 3.7 x 10^{-5}$

The range reference function $h_{rf}(\tau)$ and every row data of $S_{\sigma b}(m, n)$ are transformed to frequency domain by using Fourier transformation. Each row of the transformed signal is then multiplied with the range matched filter and the result is transformed to time domain data array $S_{\sigma c1}(m, n')$, where $n' = 1, 2, 3, \ldots, 2048$, using inverse range FFT. Figure 4.18 shows the image of the range compressed data array $S_{\sigma c1}(m, n')$ which appear in range azimuth. The range-compressed data array $S_{\sigma c1}(m, n')$ is transformed to rang Doppler frequency domain (t, ω_{dp}), by applying Fourier transform on each column of the range compressed data array $S_{\sigma c1}(m, n')$.

range Doppler Domain after range compression
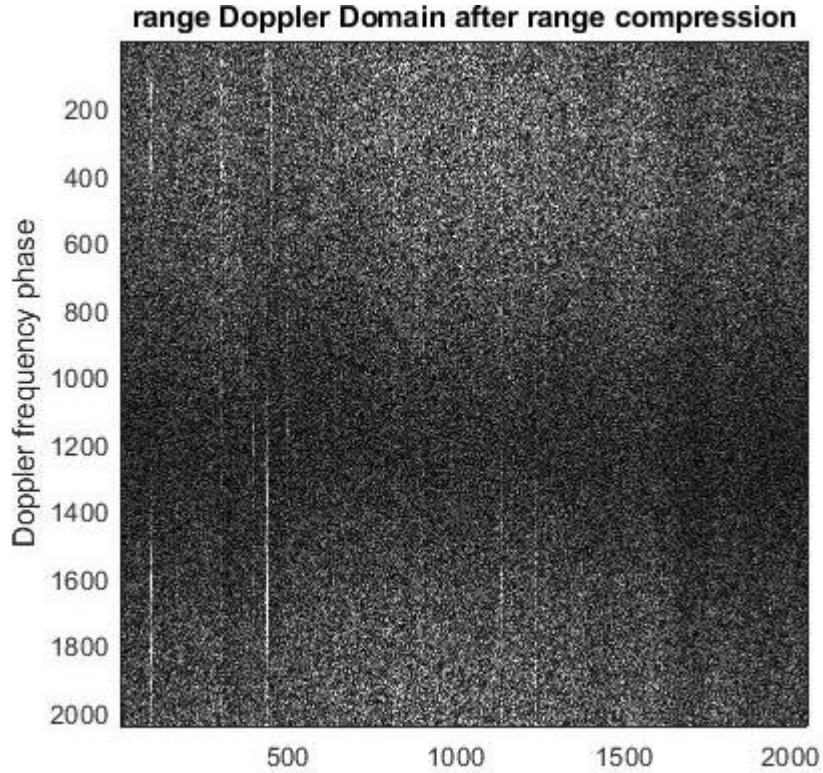
Figure 4.18. Range-compressed signal

The compressed data will then be processed by Stolt interpolation based on wavenumber domain.

Stolt interpolation starts by performing bulk azimuth compression using 1D and 2D azimuth matched filter and then applying differential azimuth compression. Since the ERS data provided is from broadside SAR, the 2D azimuth reference function is approximated to 1D reference function $H_{af}(\omega_{dp})$.

The compressed data in range Doppler frequency domain (t, ω_{dp}) is transformed to (ω, ω_{dp}) domain by applying FFT on each row of $S_{\sigma c1}(m, n)$ to get $S_{\sigma c1}(m', n)$ where $m' = 1, 2, 3, . . ., 2048$. The 1D azimuth reference function is then applied to $S_{\sigma c1}(m', n)$ to obtain a roughly compressed signal $S_{\sigma c2}(m, n)$ in (ω, ω_{dp}) domain. Applying a 2D inverse FFT on the bulk compressed data $S_{\sigma c2}(m, n)$, a roughly constructed image

64

$I_\sigma(m, n)$ with respect to $\omega, and\ \omega_{dp}$ is obtained. Figure 4.19 displays the roughly constructed image $I_\sigma(m, n)$ of Stolt interpolation technique.
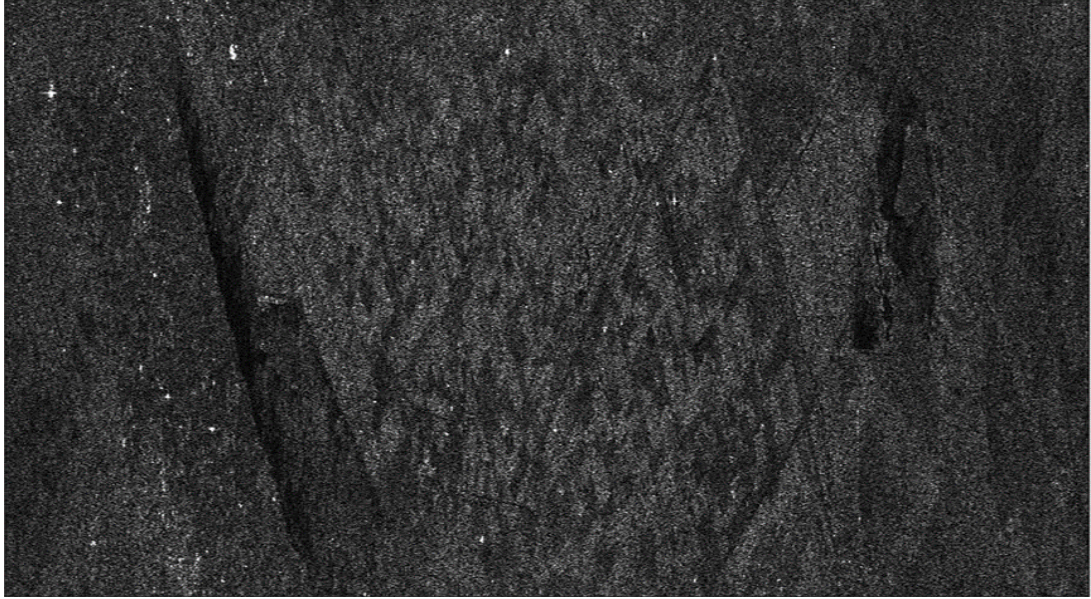
Figure 4.19. Processed image by Stolt interpolation technique without DAC

Comparing 4.19 by Stolt interpolation technique without DAC and 4.13 by RDA, it can be seen that the two algorithms generate images which are difficult to differentiate in terms of have quality (having similar quality). The quality of the roughly compressed image of figure 4.19 can further be improved by applying differential azimuth correction (DAC).

The bulk compressed data array $S_{\sigma c2}(m, n)$ in (ω, ω_{dp}) domain is inversely Fourier transformed to range Doppler frequency domain (t, ω_{dp}) before applying differential azimuth correction . To design the [13] differential azimuth correction function, the range difference Δx_n and the phase constant k_{mc} are computed as:

$$\Delta x_n = c\left(\frac{n - N_r}{f_s}\right) \quad \text{and} \quad k_{mc} = \frac{1}{4}\left(\frac{k_y^2}{k_c}\right)$$

Where $k_y = 2\pi m f_{PRF}/VN_y$, $k_c = 2\pi f_c/c$, m = 1, 2, 3, . . ., N_y, $N_y = 2048$, n = 1, 2, 3,. . ., N_x, and the reference sample N_r , equals to the range value corresponding to the slant range R_0 (or the range sample value at X_c).

The differential azimuth function is applied on the compressed data $S_{\sigma c2}(m, n)$ for the whole range samples from 1 to 2048 as in the equation form:

$$I_{\sigma a}(m, n) = S_{\sigma c2}(m, n) \ \exp(-i * k_{mc} * \Delta x_n.)$$

After differential azimuth compression is computed on the roughly constructed image $I_\sigma(m, n)$, then inverse Fourier Transform is applied on $I_{\sigma a}(m, n)$ to obtain the final constructed image as shown in figure 4.20.
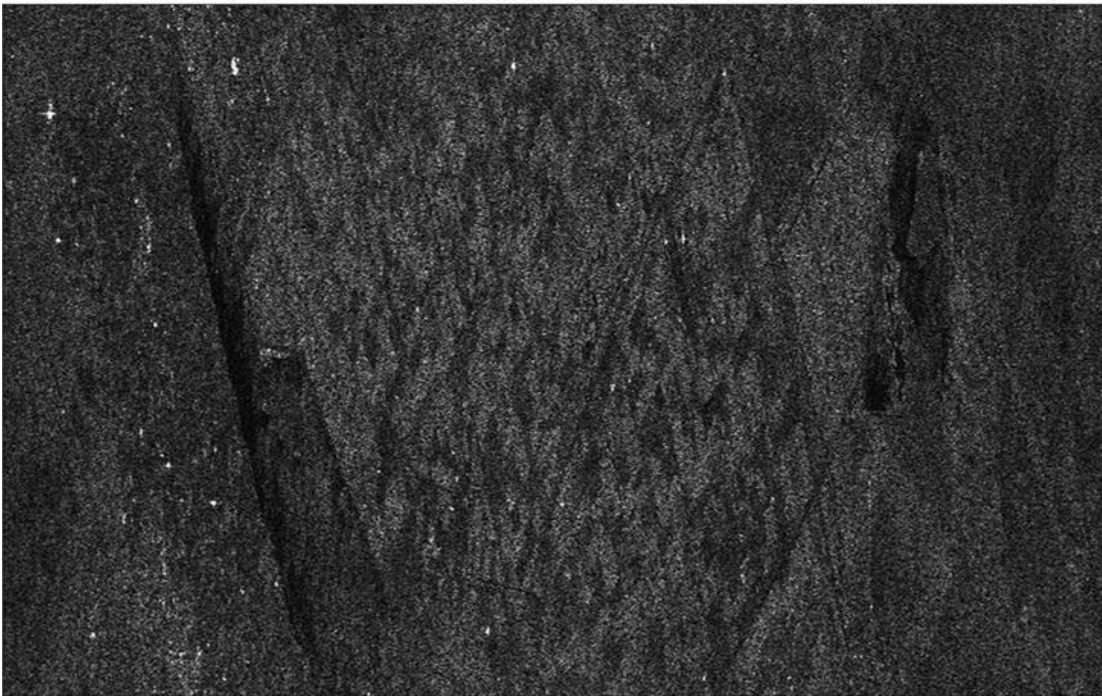
Figure 4.20. Processed SAR image

Comparing the two constructed images of 4.19 and 4.20 the constructed image figure 4.20 improves slightly in quality.

4.3. Chirp Scaling Processing

The chirp scaling algorithm is widely used because it's simple and easy to implementation as compared to algorithms that that require sophisticated interpolations. This algorithm is needed for systems that transmits high bandwidth of signal. Chirp scaling algorithm can

operate in both 2D dimensional frequency domain and in range Doppler domain. In chirp scaling algorithm, the total range curvature (RCM) is divided into the differential RCM which is range dependent and the bulk RCM which is range independent. The differential RCM is the variation in range curvature over the scanned area. The differential RCM and the bulk RCM are corrected separately. The range curvature of all the targets in the data are made uniform by the Chirp scaling algorithm. The bulk RCM is corrected by a phase multiplication whereas the differential RCM is corrected by chirp scaling operation.

4.3.1. Chirp scaling operation

This is multiplying the range chirp in the SAR raw data with a low FM rate chirp. The SAR raw data is first transform to Range-Doppler domain by taking azimuth FFT, before it is multiplied with the chirp scaling reference function. Also the phase of the chirp scaling operator represents a chirp waveform but with lower chirp rate as compared to that of the radar transmitted signal [19]. The chirp scaling operator modifies the range scaling factor by slightly increasing the chirp rate of all the signal [19], [10] and adds a linear phase that increases with the target distance from the scene centre. In the range reference function operation, the linear phase components added by the chirp scaling operator, shifts the range location of a point target response nearer to the scene centre and the size of this shift increases linearly with target's distance target distance from the scene centre. The overall result is that chirp scaling factor modifies the range scaling factor that turn to equalizes curvature arcs and also chirp scaling operation introduces a range dependent phase term for the next step of chirp scaling algorithm easily removes. Both the amount of chirp scaling and its corresponding change in range scaling factor vary approximately with azimuth frequency to force all targets to have the same range curvature as that of the target at the selected reference range. This reference range is usually selected as the broad side range to scene Centre [19].

The expression of SAR data in Range-Doppler domain is shown in equation 4.26

$$S(\tau, f_{az}; r_0) = \mathcal{C}W_{ra}\left(\tau - \frac{2R(f_{az};r_0)}{c}\right) * W_{az}\left(-\frac{r_0 f_{az}\lambda}{2V^2 b_0(f_{az})}\right) * \exp\left\{-j\pi K(f_{az})\left[\tau - \frac{2R(f_{az};r_0)}{c}\right]^2\right\} *$$

$$\exp\left\{j\frac{4\pi}{\lambda}r_0 b_0(f_{az})\right\} \qquad\qquad\qquad 4.26$$

Where $\mathcal{C}$ is a complex constant, W_{ra} is the envelope of the transmitted range pulse, W_{az} is the two way azimuth antenna pattern, V is the velocity of the radar sensor, λ is the wavelength of the carrier signal, r_0 is the closest approach distance, τ is the time in range direction, c is the speed of light, $K(f_{az}; r_0)$ is the modified modulation rate of the chirp signal and f_{az} is the azimuth frequency which varies within the range

$$-\frac{prf}{2} + f_{dc} \leq f_{az} \leq f_{dc} + \frac{prf}{2}$$

Where prf is the pulse repetition frequency and f_{dc} is the Doppler frequency at the beam Centre. The first and second phase functions in equation 4.26 is the modulated signal in range direction and the modulated signal in frequency domain in azimuth direction respectively. $R(f_{az}; r_0)$, is the range migration in the range time and azimuth frequency domain. The range migration $R(f_{az}; r_0)$, is given as;

$$R(f_{az}; r_0) = \frac{r_0}{b_0(f_{az})} = r_0(1 + a_0(f_{az}))$$

The modified modulation rate $K(f_{az})$ is derived for negative values of the modulation rate of the transmitted chirps k_r and the approximation factor $b_0(f_{az})$ as;

$$\frac{1}{K(f_{az}; r_0)} = \frac{1}{k_r} - \frac{2\lambda r_0\left(b_0^2(f_{az}) - 1\right)}{c^2 b_0^3(f_{az})}$$

Where the approximation factor

$$b_0(f_{az}) = \sqrt{1 - \frac{f_{az}^2 \lambda^2}{4V^2}}$$

The chirp scaling factor $a_0(f_{az})$ and the scaled chirp scaling factor $a_{scf}(f_{az})$ are given as:

$$a_0(f_{az}) = \frac{1}{b_0(f_{az})} - 1$$

68

and $\quad a_{csf}(f_{az}) = a_0(f_{az}) + (1 + \alpha_r) \cdot \frac{(1 + a_0(f_{az}))}{\alpha_r}$

where α_r is the additional scaling factor in the range direction.

4.3.2. Reconstruction Algorithm for Chirp Scaling Processing

The block diagram of the chirp scaling algorithm is sown on figure 4.15.

1) The raw-data is transformed into range Doppler domain with an azimuth FFT. In the Range-Doppler domain, the chirp scaling phase function H_{k1}, is obtained as:

$$H_{k1}(f_{az}, \tau) = exp\left[-j\pi a_{csf}(f_{az}) \mathbb{K}(f_{az}; r_{rf}) \left(\tau - \frac{2R(f_{az}; r_{rf})}{c}\right)^2\right]$$

Where r_{rf} is the reference range.

The chirp scaling operator is then multiplied with the signal in the Range-Doppler domain using a phase multiply. After applying H_{k1} filter, the differential RCM gets corrected.

2) After applying chirp scaling operator, the SAR data is transformed into 2D frequency domain by applying a range FFT to the data. A phase multiply is performed with the H_{k2} filter to compress the data in range. The range compression, Secondary range compression (SRC) and the bulk RCM are incorporated in the same operation and are done in the 2D frequency domain of the data. The filter H_{k2} which performs the three operations is given as:

$$H_{k2}(f_{az}, f_{rn}) = exp\left[-j\pi \frac{(f_{rn})^2}{\mathbb{K}(f_{az}; r_{rf})(1 + a_{csf}(f_{az}))}\right] \cdot exp\left(j\frac{4\pi}{c} a_0(f_{az}) r_{rf} f_{rn}\right)$$

Where f_{rn} is the range frequency. After applying the H_{k2} filter in the 2D frequency domain, the range compression, secondary compression and the bulk RCMC are completed. After this operation the data is transformed back to range Doppler domain by applying range inverse FFT to the data.

69
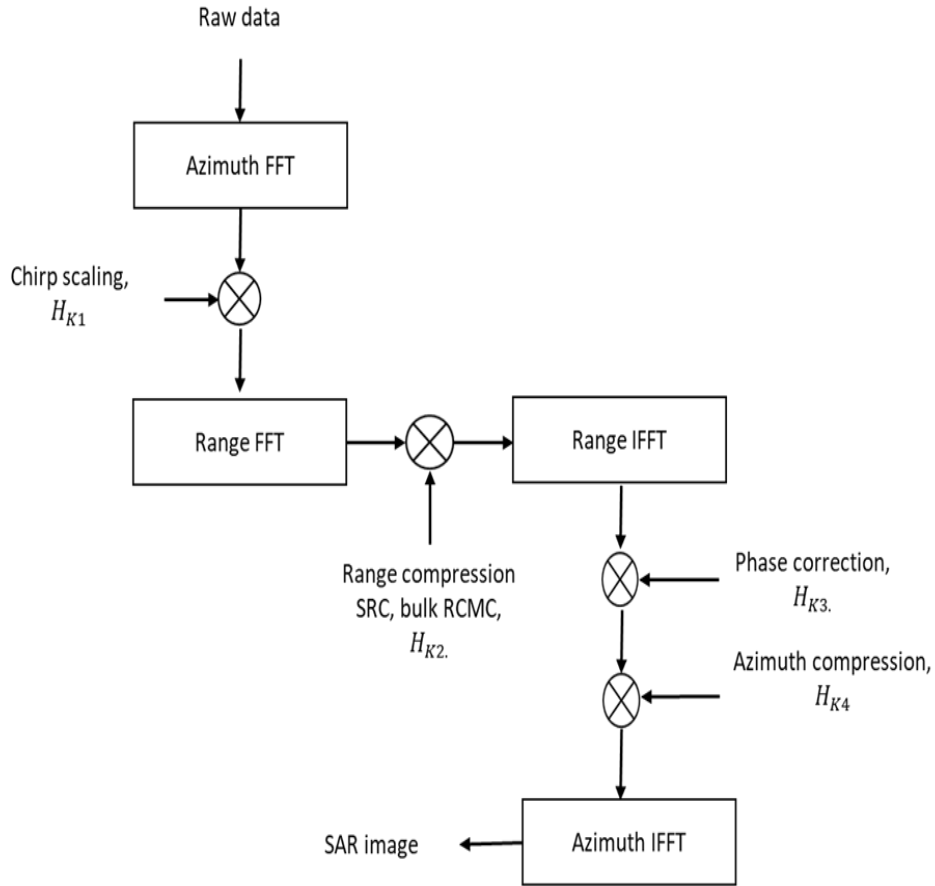
Figure 4.20 . Block diagram of chirp scaling algorithm

3) Next a phase correction is required due to the chirp scaling operation. The residual phase present in the data are corrected by applying the filter H_{k3} in the Range-Doppler domain at this stage. The H_{k3} filter at this stage is given as:

$$H_{k3} = exp\left[j4\pi \frac{a_{csf}(f_{az})K(f_{az}; r_{rf})(1 + a_0(f_{az}))^2}{c^2\left(1 + a_{csf}(f_{az})\right)}(r_0 - r_{rf})^2\right]$$

After applying H_{k3} filter in the Range-Doppler domain, the residual phase is corrected.

After phase correction, the azimuth compression is done in the Range-Doppler domain. The H_{k4} filter required to perform the azimuth compression at this stage is given as:

70

$$H_{k4}(f_{az}) = exp\left[j\frac{4\pi}{\lambda}r_{0scf}(b_0(f_{az})-1)\right]$$

Where $r_{0scf} = r_{rf} + \frac{(r_0 - r_{rf})}{\alpha_r}$

After multiplying the data with the H_{k4} filter in Range-Doppler domain, the azimuth compression is completed and the resulting range-Doppler domain azimuth compressed data is inversely Fourier transform back into time domain which is the desired SAR image.

4.3.3. Reconstruction of Satellite Radar Image using Chirp Scaling Algorithm.

In this section, a satellite-based (ERS) raw data generated by ESA, processed and distributed by German Aerospace Center, DLR will be used in reconstructing the radar image using Chirp Scaling Algorithm. The parameters of the sensor are listed on table 4. Figure 4.21 shows the ERS raw data set to be processed using the Chirp scaling algorithm
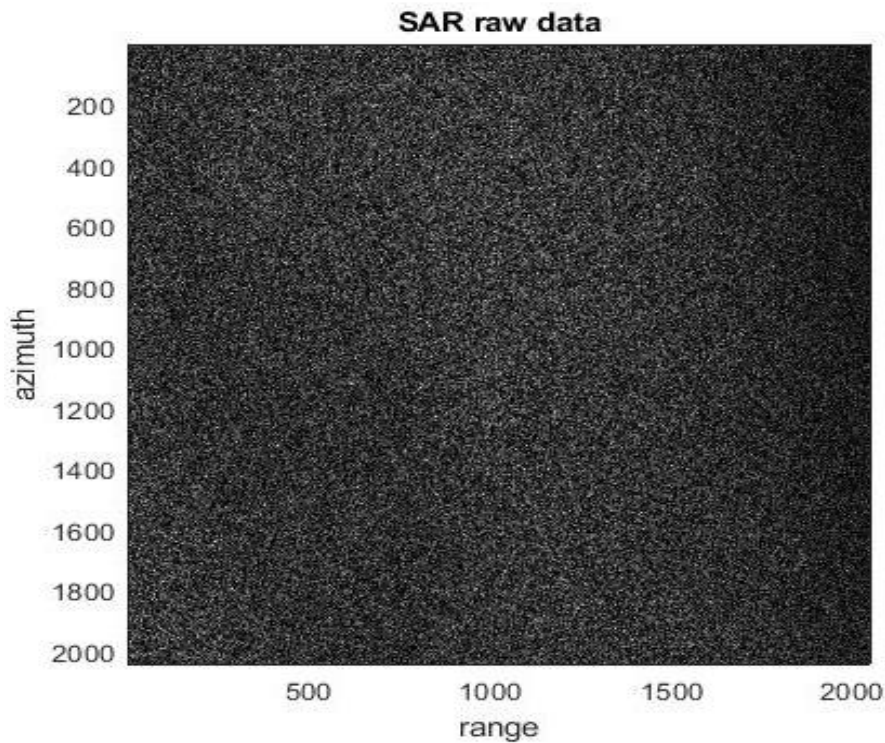
Figure 4.21 ERS data set

71

To process this data using chirp scaling algorithm, the data set is first transformed into the Range Doppler domain by computing azimuth FFT. That is, the data is first transformed from azimuth time to Doppler frequency. The expression of SAR data $S(\tau, f_{az}; r_0)$, in Range-Doppler domain can be seen in equation 4.26. The azimuth chirp scaling is achieved by applying the chirp scaling phase multiplication using the chirp scaling function $H_{k1}(f_{az}, \tau)$ on the data $S(\tau, f_{az}; r_0)$.

$$S_1(\tau, f_{az}; r_0) = S(\tau, f_{az}; r_0) * H_{k1}(f_{az}, \tau)$$

Figure 4.22 shows the azimuth chirp scaling and range scaling data obtained after applying the chirp scaling phase multiplication.
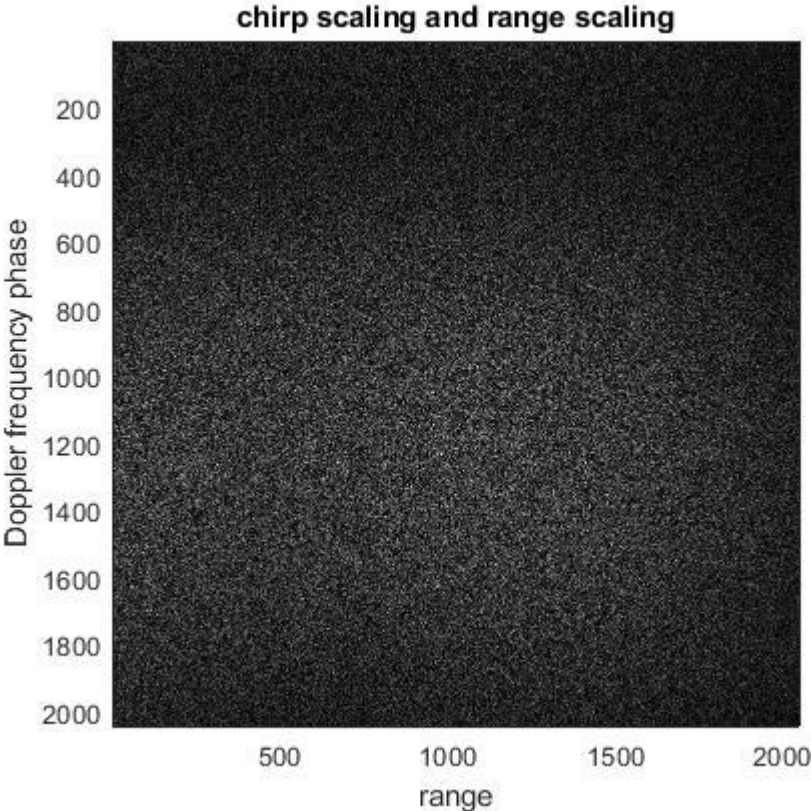
Figure 4.22. azimuth chirp scaling and range scaling data

After the operation of chirp scaling phase multiplication, the resulting phase-history data which is in azimuth-frequency domain is transform to range-frequency domain

$S_1(\tau, f_{az}; f_{rn})$ by applying range FFT. The data now is in two dimensional frequency domain, that is in azimuth frequency and range frequency domain. In the second phase multiplication, the 2D range match filter $H_{k2}(f_{az}, f_{rn})$ that depends on both azimuth and range is applied to all the range frequencies in the data with a dependence on f_{rn}.

$$S_2(\tau, f_{az}; f_{rn}) = S_1(\tau, f_{az}; f_{rn}) * H_{k2}(f_{az}, f_{rn})$$

After applying the H_{k2} filter in the 2D frequency domain, the range compression, secondary compression and the bulk RCMC are completed. Figure 4.23 displays the resulting data after the bulk rcmc and range compression
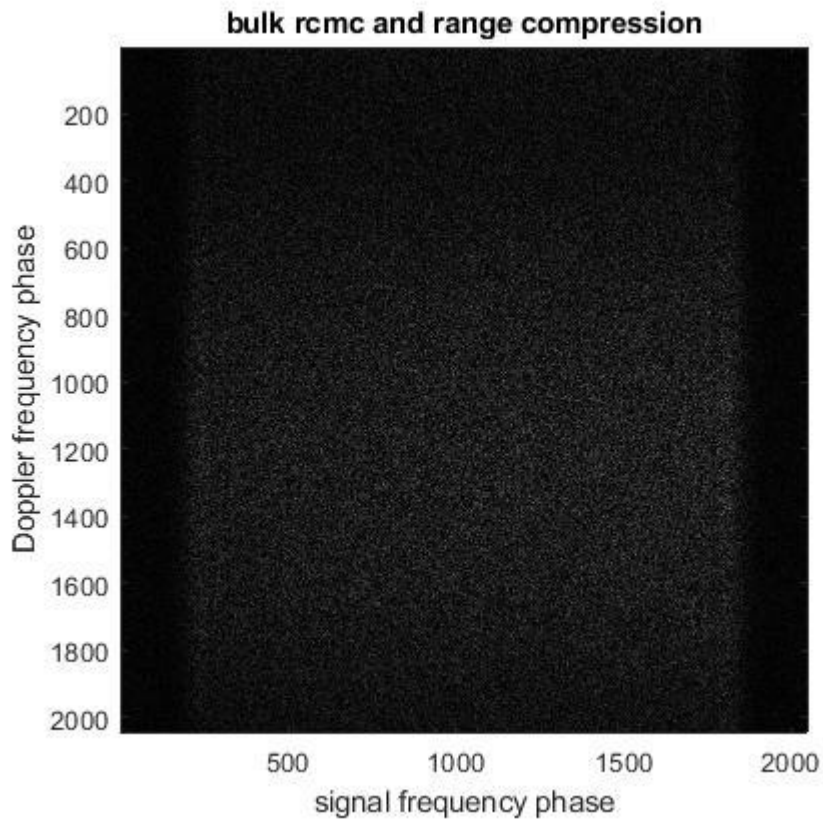
Figure 4.23 Bulk RCMC and Range compressed data

After compressing the signal in range, the range compressed signal $S_2(\tau, f_{az}; f_{rn})$ is returned to range Doppler domain $S_2(\tau, f_{az}; r_0)$ by computing 1-D inverse FT of $S_2(\tau, f_{az}; f_{rn})$. Figure 4.24 shows the range compressed data

After the range compression, the range curvature is corrected for all targets in the scene. At this stage, the residual phase due to the chirp scaling operation (first phase correction) are corrected by applying the filter H_{k3} in range Doppler domain to the range compressed data.

$$S_3(\tau, f_{az}; r_0) = S_2(\tau, f_{az}; r_0) * H_{k3}(f_{az}, r_0)$$
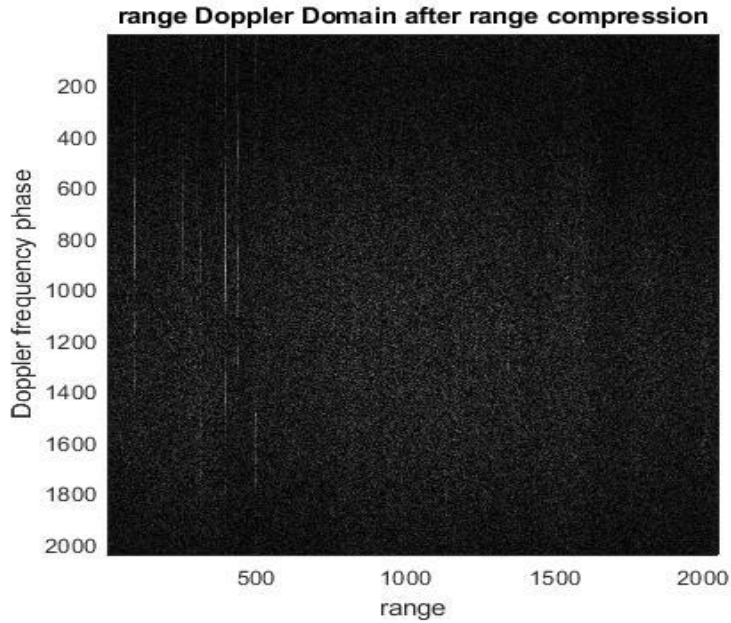
Figure 4.24 Compressed data in range Doppler domain

After applying H_{k3} filter in the Range-Doppler domain, the residual phase is corrected and the residual phase is corrected data is shown in 4.25. After phase correction, the third phase multiplication is the azimuth compression in the Range-Doppler domain. Azimuth compression is done by applying the range dependent azimuth matched filter $H_{k4}(f_{az})$ on the range Doppler domain residual phase is corrected data.

$$S_4(\tau, f_{az}; r_0) = S_3(\tau, f_{az}; r_0) * H_{k4}(f_{az})$$

After applying the $H_{k4}(f_{az})$ filter, the resulting azimuth compressed data in Range Doppler domain can be seen in figure 4.26.
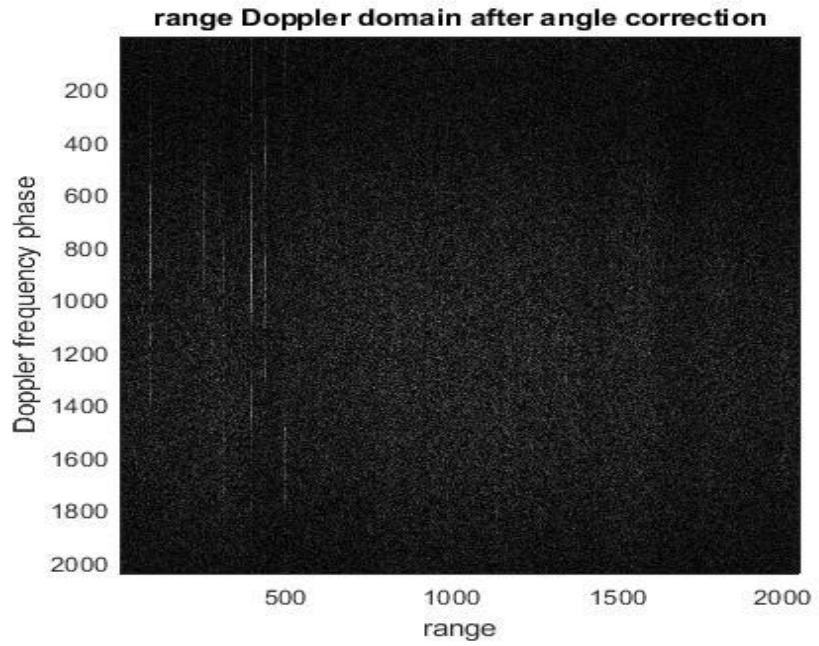
Figure 4.25. Residual phase is corrected data
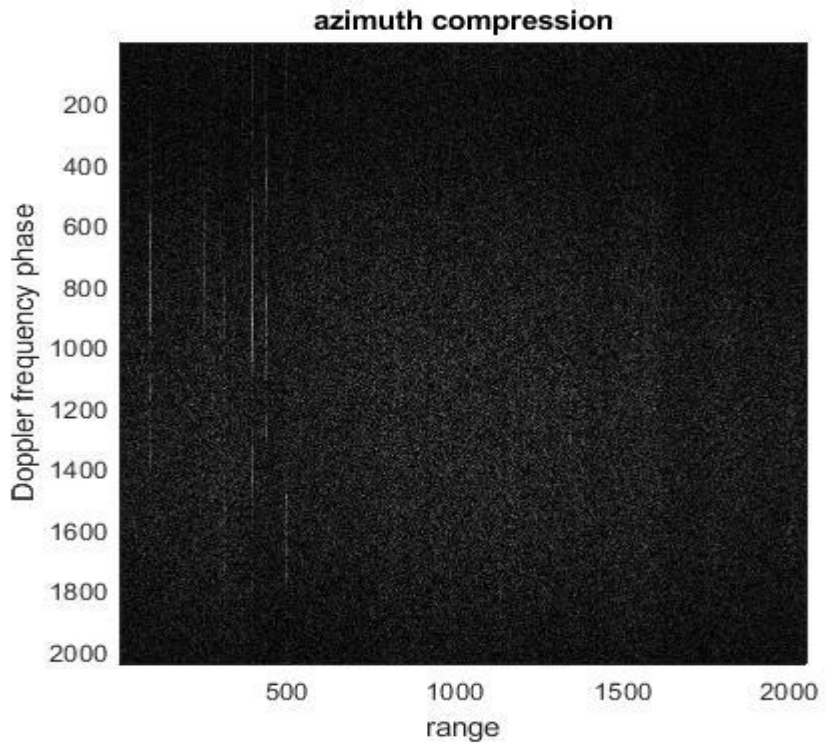
Figure 4.26. Azimuth compressed data in Range Doppler domain

75

After applying the range dependent azimuth matched filter, the azimuth compression is completed by taking 1D inverse FT and the resulting data is now compressed in both the range and the azimuth resulting to a single look complex image as shown in 4.27.
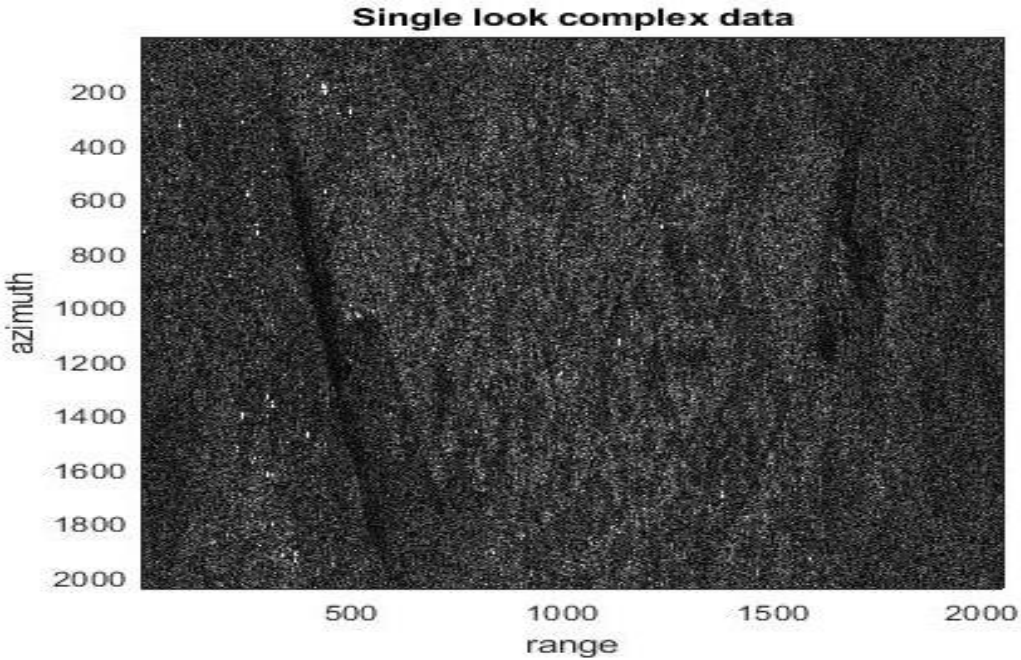
Figure 4.27. Single look Complex image

As the Single look complex image in figure 4.27 is highly speckled. To reduce the speckle effect on the processed image, a multilook and spatial filtering is applied on the image. Figure 4.28 display the multilooked and spatial filtered image.
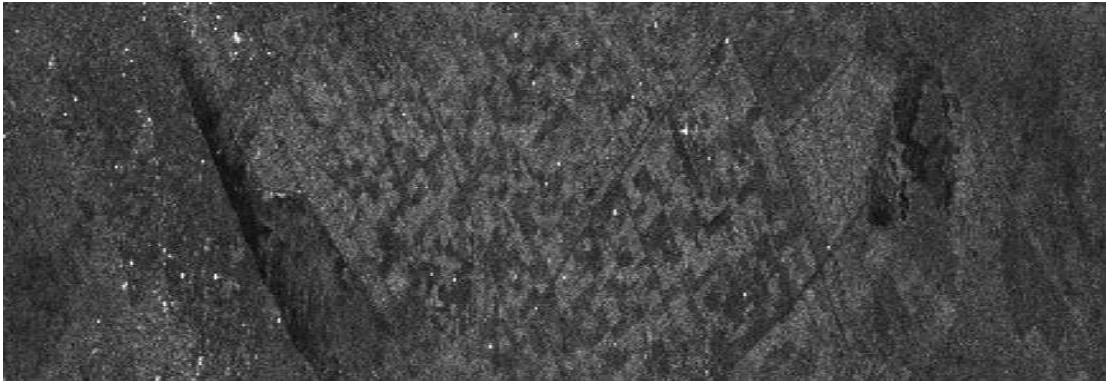
Figure 4.28. Multilooked and spatial filtered image

76

5. CONCLUTION

This work focuses on the Range-Doppler technique, Stolt Interpolation technique and the chirp scaling technique in detail and their respective flow diagrams and important parameter expressions has been described in detailed. Also, the Range-Doppler technique, Stolt Interpolation technique and the chirp scaling technique were successfully implemented on Matlab to construct the SAR image and the three algorithms were compared as follows;

The Range-Doppler algorithm is computationally efficient, flexible, accurate, and less computational time in processing radar images. It has some disadvantages with respect the high computational time to obtain good accuracy when range cell migration correction operation is involved. That is, it becomes computationally heavy when an accuracy is required in computing range cell migration correction.

The Stolt interpolation algorithm is very accurate but computationally intensive due to heavy interpolation involved. It has advantages over the Range-Doppler algorithm.

The Chirp scaling algorithm does not use interpolation of the data. It eliminates Interpolation in RCMC. It achieves the range cell migration correction with phase multiplies instead of interpolations. It also has additional advantage that secondary range compression can be made azimuth frequency dependent which results in reduced time of computation. Data processing by Chirp Scaling algorithm takes about 15% longer that processed by Range Doppler algorithm. Due to high computational complexity, chirp scaling algorithm requires higher of memory.

6. REFERENCES

[1] **E. Podest,** Basics of Synthetic Aperture Radar," National Aeronautics and Space Administration", 29 November 2017.

[2] **C. Lopez-MARTINEZ**, "Models and Information in Multichannel radar Remote Sensing Imagery," IGARSS, Catalunya, 2007.

[3] **Stefan AUER**, "German Aerospace Center, DLR," 2000. [Online]. Available: https://saredu.dlr.de/unit/SAR_imaging.

[4] **D. Jenn**, "Naval Post Graduate School-Radar Fundamentals," [Online]. Available: http://www.nps.navy.mil/faculty/jenn.

[5] **A. M. Younis,** "A Tutorial on Synthetic Aperture radadar" Microwaves and Radar ,Institute of the German Aerospace Center (DLR), IEEE **Geoscience and Remote Sensing Magazine**, Germany, 17 April 2013.

[6] **CHEN AND KUNSHAN**, **Principles of Synthetic Aperture Radar Imaging**: A System, Boca Raton,: CRC Press, Taylor & Francis Group, 2016, p. 1.

[7] **N. Dastgir**, "Processing SAR data using Range Doppler and Chirp Scaling Algorithms," School of Architecture and Built Environment Royal Institute of Technology , Stockholm, April 2007.

[8] **C. R. Jackson**, "Principles of synthetic Aperture radar" radar imaging resources," Alexandria, VA USA..

[9] **A. Moreira**, "Synthetic Aperture Radar (SAR): Principles and Applications," German Aerospace Center (DLR), Microwaves and Radar Institute, Germany, July, 2013.

[10] **Walter G. Carrarra**, **Spotlight Synthetic Aperture Radar Signal Processing Algorithms**., Boston: Artech House.

[11] **TEO Long**, "Geosynchronous SAR: System and Signal Processing," Springe*r* Science and Business media LLC, 2018.

[12] **M. Henri,** "Processing of Synthetic Aperture Radar," SAR images Digital and Image processing Series, 2008.

[13] **BU-Chin Wang**, **Digital Signal Processing Techniques and Application in Radar Image Processing**, Hoboken, New Jersey: A JOHN WILEY & SONS, INC.,, 2008.

[14] **M. A. Richards**, "Fundamentals of Radar Signal Processing," McGraw-Hill, New York, 2005.

[15] **J. C. Curlander**, **Synthetic Aperture Radar systems and Signal processing**, USA: John Wiley & Sons, Inc, 1991.

[16] **BU-chin Wang**, "Range-Doppler Processing on SAR Images," in **Digital Signal Processing Techniques and Applications in Radar Image Processing** 01/29/2008.

[17] **I. D. K. Voon-Chet,** "Radar Signal processing using matlab," Business Development Manager, iRadar Sdn Bhd.

[18] **M. Soumekh**, **Synthetic Aperture Radar Signal Processing with Matlab algorithms**, Canada: John Wiley & Sons Inc, 1999.

[19] **S. C. Satapathy**, "Advances in Decision Sciences, Image Processing, Security and Computer Vision," in Springer Nature Switzerland AG, Switzerland, 2020.

[20] **Y. D. Robert Wang**, **Bistatic SAR System and Signal Processing Technology**, Singapol: Springer , 2018.

[21] **J. A. S. William L. Melvin**, "Stripmap SAR," in **Principles of Modern Radar Advanced techniques**, New York, SciTech Publishing, an imprint of the IET, , 2013.

[22] **H. Wu**, "Motion Compensation for Near-Range Synthetic Aperture Radar Applications," KIT Scientific Publishing, 2012.

[23] **B. M. Charbit**, **Digital Signal and Image Processing Using MATLAB**, USA: John Wiley & Sons, Inc., July 22, 2014.

[24] **A. Moreira,** "Chirp Scaling Algorithm for processing SAR data with high squint angle and motion error," German Aerospace Research Establishment (DLR), Oberpfaffenhofen, Germany, 1994.

[25] **David Sandwell**, "SAR Image Formation: ERS SAR Processor coded in Matlab," John Wiley & Sons, 2008.

[26] **A. Hein**, "Processing of SAR Data, Fundamentals, Signal Processing, Interferometry," Springer-Verlag, Berlin Heidelberg, 2004.

[27] **C. P. Xinning**, "An imaging algorithm for multiple receiver synthetic aperture sonar," in IEEE 2nd Advanced Information Technology, Electronic and Automation Control Conference (IAEAC), 2017.

[28] **D. Massonnet**, **Imaging with Sythetic Aperture RADAR**, Lausanne, Switzerland: Taylor and Francis Group, LLC, 2008.

[29] **F. Adragna**, "Synthetic Aperture Radar Images", in Processing of Sythetic Aperture Radar Images, Paris, Wiley, 2008.

[30] **I. C. Davidson**, "Signal properties of space borne squint-mode SAR," IEEE Transactions on Geoscience and Remote Sensing, 1997.

APPENDICES

Appendix: A MATLAB code for Range Doppler Algorithm

```matlab
tic;

% ERS satellite Sensor parameters

fs=18.962468*10^6;                    % Range Sampling Frequency [Hz]
K_r=4.18989015*10^(11);               % FM Rate Range Chirp [1/s^2]
tau_p=37.12*10^(-6);                  % Chirp duration [s]
V=7098.0194;                          % Effective satellite velocity [m/s]
lambda=0.05656;                       % Length of carrier wave [m]
R_0=852358.15;                        % Range to center of antenna footprint
t_a=0.6;                              % Aperture time [s]
prf=1679.902;                         % Pulse repetition Frequency [Hz]

%  Load ERS raw data

data = load('ERS.mat');

% Get data size

fn = fieldnames(data);
raw_data = getfield(data, fn{1});
Naz = size(raw_data,1);               % Azimuth size
Nrg= size(raw_data,2);                % Range size

% Display raw data and raw data spectrum

figure;
imagesc(abs(raw_data));colormap('gray');
title('Raw data'); xlabel('Range pixels'); ylabel('Azimuth pixels');
axis equal; axis on;
figure;
imagesc(abs(fftshift(fft2(raw_data))));
title('Raw data spectrum'); xlabel('Range pixels'); ylabel('Azimuth pixels');
```

83

```matlab
axis equal; axis on;  caxis([0 10000]);


% Data File Location

OutputFile_Name='SAR Raw data';

% Definition of range matched filter
% Basic definitions

tau=-tau_p/2:1/fs:tau_p/2;                              % time axis in range
omega = -fs/2:1/tau_p:fs/2;                             % frequency axis in range

% Define range chirp in time and frequency domain

ra_cp = exp(1i.*pi.*K_r.*( -tau_p/2:1/fs:tau_p/2).^2);    % Range chirp in time domain
RA_CP = fftshift(fft(ra_cp));                             % Rananange chirp in ferquency
domain

% Display range chirp in time and frequency domain

figure;
subplot(3,1,1); plot(tau,real(ra_cp),'b');
title('Real part of Range chirp'); xlabel('Time sample [sec]'); ylabel('Amplitude');
xlim([min(tau) max(tau)]);

subplot(3,1,2); plot(tau,imag(ra_cp),'r');
title('Imaginary part of Range chirp'); xlabel('Time sample [sec]'); ylabel('Amplitude');
xlim([min(tau) max(tau)]);
subplot(3,1,3); plot(omega, abs(RA_CP),'g');
title('Spectrum of range chirp'); xlabel('Frequency bin'); ylabel('Absolute');
xlim([min(omega) max(omega)]);

% Definition of range matched filter

ra_ma_f=exp(-1i.*pi.*K_r.*(-tau_p/2:1/fs:tau_p/2).^2);     % Range matched filter
in time domain

% Apply zero padding on range matched filter in time domain

ra_ma_fter=zeros(1,Nrg);                                    % Row matrix to be filled
with chirp values
ra_ma_fter(ceil((Nrg-length(tau))/2):length(tau) + ceil((Nrg-length(tau))/2)-1)=ra_ma_f;
```

```matlab
RA_MA_FTER = fft(ra_ma_fter);                              % Range matched filter in
frequency domain

% Range compression

% Empty matrix to be filled with processed data

data=zeros(Naz, Nrg);

for r1 = 1 : Naz                                            % defining size of row
    rr = raw_data(r1,:);                                   % selecting row in raw data
    RR = fft(rr);                                          % transform into frequency domain
    RA_COMP_D = RR.*RA_MA_FTER; % multiplying spectra
    ra_comp_d = fftshift(ifft(RA_COMP_D)); % transform into time domain
    data(r1, :) = ra_comp_d;

end

clear r1 rr RR RA_COMP_D ra_com_d

% Display Range compressed data

figure;
imagesc(abs(data)); colormap('gray'); axis('image');caxis([0 600]);
xlabel('range'); ylabel('Doppler frequency phase')
title('range Doppler Domain after range compression')

% Defining Azimuth matched filter
% Basic definitions

t=-t_a/2:1/prf:t_a/2;                                      % time axis in azimuth
v=-prf/2:1/t_a:prf/2;                                      % frequency axis in azimuth

% Azimuth Chirp Rate

K_a=-2*V^2/lambda/R_0;

% Define of azimuth chirp in time and frequency domain

az_cp = exp(1i.*pi.*K_a.*(-t_a/2:1/prf:t_a/2).^2);    % time domain
AZ_CP = fftshift(fft(az_cp));                              % frequency domain

% Display azimuth chirp in time and frequency domain
```

```matlab
figure;
subplot(3,1,1); plot(t,real(az_cp),'b');
title('Real part of Azimuth chirp'); xlabel('Time sample [sec]'); ylabel('Amplitude');
xlim([min(t) max(t)]);
subplot(3,1,2); plot(t,imag(az_cp),'r');
title('Imaginary part of Azimuth chirp'); xlabel('Time sample'); ylabel('Amplitude');
xlim([min(t) max(t)]);
subplot(3,1,3); plot(v, abs(fftshift(fft(az_cp))), 'g'); title('Spectrum of azimuth chirp');
xlabel('Frequency'); ylabel('Absolute'); xlim([min(v) max(v)]);

% Definition of azimuth matched filter

az_mat_f = exp(-1i.*pi.*K_a.*(-t_a/2:1/prf:t_a/2).^2);        % azimuth matched filter in
time domain

% Apply zero padding on azimuth matched filter

az_mat_fter=zeros(1,Naz);          % Empty column to be filled with chirp values
az_mat_fter(ceil((Naz-length(t))/2): length(t)+ceil((Naz-length(t))/2)-1)=az_mat_f;
AZ_MA_FTER = fft(az_mat_fter);       % Azimuth matched filter in frequency domain

% Azimuth compression

for co = 1:Nrg                                       % defining size of column
    col = data(:,co);                                % select column in processed data
    COL = fft(col);                                  % Transform to frequency domain
    AZ_COMP_D = COL.*AZ_MA_FTER.';                   % Multipling spectra
    az_comp_d= fftshift(ifft(AZ_COMP_D));            % transform into time domain
    data(:,co) = az_comp_d;
end

 clear co col COL AZ_COMP_D az_comp_d

% Display constructed SAR image

out_put=abs(data);
figure;
imagesc(out_put);colormap('gray')
axis('image'); xlabel('Range'); ylabel('Azimuth')
title('Processed SAR data'); caxis([0 20000]);

% End processing of Raw data
toc;
save(OutputFile_Name, 'data')
```

86

Appendix: B MATLAB code for Stolt Interpolation Algorithm

```matlab
tic;

% ERS satellite Sensor parameters

c = physconst('LightSpeed');              % speed of light in vacuum
lambda=0.05656;                           % Length of carrier wave [m]
f_c = c/lambda;                           % carrier frequency
fs=18.962468*10^6;                        % Range Sampling Frequency [Hz]
K_r=4.18989015*10^(11);                   % FM Rate Range Chirp [1/s^2]
t_p=37.12*10^(-6);                        % Chirp duration [s]
V=7098.0194;                              % Effective satellite velocity [m/s]
R_0=852358.15;                            % Range to center of antenna footprint
t_a=0.6;                                  % Aperture time [s]
prf=1679.902;                             % Pulse repetition Frequency [Hz]

% Load ERS raw data

data = load('ERS.mat');

% Get data size

fn = fieldnames(data);
raw_data = getfield(data, fn{1});
Naz = size(raw_data,1);                   % Azimuth size
Nrg= size(raw_data,2);                    % Range size

% 2D Fourier Transform of the raw data

data = fft(fft(raw_data).').';

figure;
imagesc(abs(raw_data));
title('2D raw data spectrum'); xlabel('Range'); ylabel('Azimuth');

% Range matched filter conj(P_sig(omega))

tau=-t_p/2:1/fs:t_p/2;                         % time axis in range
P_sig = exp(-1i.*pi.*K_r.*( -t_p/2:1/fs:t_p/2).^2); % Range chirp in time domain
```

```matlab
% Apply zero padding on range matched filter in time domain

P_siG=zeros(1,Nrg);                            % Row matrix to be filled with chirp values
P_siG(ceil((Nrg-length(tau))/2):length(tau)+ ceil((Nrg-length(tau))/2)-1)=P_sig;
P_SIG = fft(P_siG);                            % Range matched filter in frequency domain

% Range compression

processed=zeros(Naz, Nrg);

for r = 1 : Naz                                % defining size of row
    RR = data(r,:);                            % selecting row in raw data
    COMPR_D = RR.*P_SIG;                        % multiplying spectra
    compr_d = fftshift(ifft(COMPR_D));         % transform into time domain
    processed(r, :) =  compr_d ;
end

% Display Range compressed data
figure;
imagesc(abs(processed)); colormap('gray'); axis('image');caxis([0 20000]);
xlabel('range'); ylabel('Doppler frequency phase')
title('range Doppler Domain after range compression')

% Applying 1D azimuth matched filter in slow time t
m=1008;
dt=-t_a/2:1/prf:t_a/2;                          % time axis in azimuth

% Azimuth Chirp Rate

K_a=-2*V^2/lambda/R_0;

h_af=exp(-1i*pi*K_a*(dt).^2);
figure;
subplot(2,1,1); plot(dt,real(h_af),'b');
title('Real part of Azimuth chirp'); xlabel('Time sample [sec]'); ylabel('Amplitude');
xlim([min(dt) max(dt)]);
subplot(2,1,2); plot(dt,imag(h_af),'r');

% Apply zero padding on azimuth matched filter

h_after=zeros(1,Naz);                           % Empty column to be filled with chirp values
h_after(ceil((Naz-length(dt))/2): length(dt)+ceil((Naz-length(dt))/2)-1)=h_af;
H_AFTER = fft(h_after);                         % Azimuth matched filter in frequency domain
```

```matlab
% Azimuth compression without Differential azimuth correction

for co = 1:Nrg                              % defining size of column
    col = processed(:,co);                  % select column in processed data
    AZ_COMP_D = (col.').*H_AFTER;           % Multipling spectra
    az_comp_d= fftshift(ifft(AZ_COMP_D));   % transform into time domain
    processed(:,co) = az_comp_d;
end
figure,
imagesc(abs(processed)); colormap('gray'); axis('image');
xlabel('Range'); ylabel('Azimuth')
title('roughly constructed image without DAC'); caxis([0 20000]);

clear co  col AZ_COMP_D az_comp_d

% Differential azimuth correction function

N_y=2048;
k_y = 2*pi*m*prf/V/N_y;
k_c=2*pi*f_c/c;
dx_n=c*704/fs ;
Dif_az=exp(-1i.*(k_y.^2/4/k_c).*dx_n);

% Applyinhg Differential azimuth correction

for da = 1:Nrg                              % defining size of column
    da1 = processed(:,da);                  % select column in processed data
    DA = fft(da1);                          % Transform to frequency domain
    DAC = DA.*Dif_az;                       % Multipling with DAC
    dac= ifft(DAC);                         % transform into time domain
    processed(:,da) = dac;
end
figure,
imagesc(abs(processed)); colormap('gray'); axis('image')
xlabel('Range'); ylabel('Azimuth')
title('Processed image with DAC'); caxis([0 20000]);

% Applying multi-look processing and spatial filtering

% Multilooking on/off
multilook = 1;                              % 0: no; 1: yes
m_factor = 10;                              % multilooking factor (spatial)
```

```matlab
if multilook == 1

    % define size of output image
    output_image=zeros(ceil(Naz/m_factor),Nrg);

    % Dummy index
    index=1;

    % Spatial averaging
    for i=1:m_factor:Naz-m_factor              % jump along azimuth axis according to
multilooking factor
        cor=processed(i:i+(m_factor-1),:);      % select azimuth bins
        m_cor=mean(abs(cor),1);                 % average value of azimuth bins
        output_image(index,:)=m_cor;
        index=index+1;
    end

    % Final SAR image (multi-looked)
    processed = output_image;

end

%. Display filtered image

% Display constructed SAR image

out_put=abs(processed);
figure;
imagesc(out_put);colormap('gray')
axis off; xlabel('Range'); ylabel('Azimuth')
title('Multilook SAR data'); caxis([0 15000]);
toc;

% End
```

Appendix: C MATLAB code for Chirp Scaling Algorithm

```matlab
tic;

% system parameters:

c = physconst('LightSpeed');                % speed of light in vacuum
lambda=0.05656;                             % Length of carrier wave [m]
f_c = c/lambda;                             % carrier frequency
f_s = 18.962468*10^6;                       % data sampling rate
echoes = 2048;                              % number of radar echoes in data file
samples = 2048;                             % number of samples per radar echo
near_range=829924.365777;                   % distance to the first range bin
t_near = (2*near_range)/c;                  % near range fast time (2 x range)
tau = t_near:1/f_s:t_near+samples/f_s-1/f_s; % fast time
f_dc = 0;                                   % Doppler centroid (squint angle)
v = 7098.0194;                              % SAR satellite platform velocity
PRF = 1679.902394;                          % pulse repetition frequency
t_p = 3.712e-05;                            % chirp pulse duration
k_r=-4.18989015*10^(11);                    % FM Rate Range Chirp [1/s^2]

% Additional paramters

alpha = 1;
r_ref = (tau(1)+samples/2/f_s)/2*c;
f_r = -f_s/2:f_s/samples:f_s/2-f_s/samples;
f_a = -PRF/2+f_dc:PRF/echoes:f_dc+PRF/2-PRF/echoes;

% Load ERS raw data

data = load('ERS.mat');

% Get data size

fn = fieldnames(data);
raw_data = getfield(data, fn{1});
Naz = size(raw_data,1);                     % Azimuth size
Nrg= size(raw_data,2);                      % Range size

% Display SAR Raw data

figure;
```

```matlab
imagesc(abs(raw_data)); colormap('gray'); axis('image');axis on
xlabel('range'); ylabel('azimuth'); title('SAR raw data')

% Azimuth fft

processed = ftx(raw_data);

% Applying chirp scaling, Range scaling: H_k1

beta = (1 - (f_a*lambda/2/v).^2).^0.5;
a = 1./beta - 1;
R = r_ref./beta;
a_scl = a + (1-alpha).*(1+a)./alpha;
k_inv = 1./k_r - (2.*lambda.*r_ref.*(beta.^2-1))./(c^2.*beta.^3);
k = 1./k_inv;

x = k.*a_scl;
X = x(:)*ones(1,samples);
Tau = ones(echoes,1)*tau;
y = 2.*R./c;
Y = y(:)*ones(1,samples);
Z = (Tau-Y).^2;
H_k1 = exp(-1i*pi*X.*Z);

processed = processed .* H_k1;

    figure;
    imagesc(abs(processed)); colormap('gray')
    axis('image');axis on
    xlabel('range'); ylabel('Doppler frequency phase')
    title('chirp scaling and range scaling')

% Range FFT

processed = fty(processed);

figure;
imagesc(abs(processed)); xlabel('signal frequency phase'); ylabel('Doppler frequency
phase');  title('2D spectral domain')
axis('image'); axis on

% Bulk RCMC, Range compression: H_k2

x = 1./(k.*(1+a_scl));
```

```matlab
X = x(:)*ones(1,samples);
y = f_r.^2;
Y = ones(echoes,1)*y;
z = f_r;
Z = ones(echoes,1)*z;
A = a(:)*ones(1,samples);
Z = Z .* A;
H_k2 = exp(-1i*pi*X.*Y) .* exp(1i*4*pi*r_ref/c.*Z);
processed = processed .* H_k2;

   figure;
   imagesc(abs(processed)); colormap('gray');
   axis('image');axis on
   xlabel('signal frequency phase')
   ylabel('Doppler frequency phase')
   title('bulk rcmc and range compression')

% Range inverse FFT

processed = ifty(processed);
   figure;
   imagesc(abs(processed)); colormap('gray');
   axis('image');axis on
   xlabel('range'); ylabel('Doppler frequency phase')
   title('range Doppler Domain after range compression')

% Angle correction: H_k3

r_0 = tau/2*c;
x = k.*a_scl.*(1+a).^2 ./ (c^2.*(1+a_scl));
X = x(:)*ones(1,samples);
z = (r_0-r_ref).^2;
Z = ones(echoes,1)*z;
dphi = 4*pi*X.*Z;
H_k3 = exp(1i*dphi);
processed = processed .* H_k3;
   figure;
   imagesc(abs(processed)); colormap('gray');
   axis('image');axis on
   xlabel('range'); ylabel('Doppler frequency phase')
   title('range Doppler domain after angle correction')

% Azimuth compression: H_k4
```

```matlab
r_0_scl = r_ref + (r_0-r_ref)/alpha;
X = ones(echoes,1)*r_0_scl;
Z = (beta(:)-1)*ones(1,samples);
H_k4 = exp(1i*4*pi/lambda*X.*Z);
processed = processed .* H_k4;
    figure;
    imagesc(abs(processed)); colormap('gray');
    axis('image');axis on
    xlabel('range')
    ylabel('Doppler frequency phase')
    title('azimuth compression')




% Azimuth inverse FFT

processed = iftx(processed);

% write result

figure;
    imagesc(abs(processed)); colormap('gray');
    axis('image');axis on
    xlabel('range')
    ylabel('azimuth')
    title('Single look complex data'); caxis([0 20]);

% applying multi-look processing and spatial filtering
% Multilooking on/off
multilook = 1;                                      % 0: no; 1: yes
m_factor = 10;                                      % multilooking factor (spatial)
if multilook == 1

    % define size of output image
    output_image=zeros(ceil(Naz/m_factor),Nrg);

    % Dummy index

    index=1;

    % Spatial averaging
```

94

```matlab
    for i=1:m_factor:Naz-m_factor                    % jump along azimuth axis according
to multilooking factor
        cor=processed(i:i+(m_factor-1),:);           % select azimuth bins
        m_cor=mean(abs(cor),1);                      % average value of azimuth bins
        output_image(index,:)=m_cor;
        index=index+1;
    end

    % Final SAR image (multi-looked)
    processed = output_image;

end

% write result after multi-look processing and spatial filtering

out_put=abs(processed);
figure;
imagesc(out_put);colormap('gray'); axis on
xlabel('Range'); ylabel('Azimuth')
title('multilooked and spatial filtered image'); caxis([0 15]);

toc;
```

<div align="center">END</div>

RESUME

Name and Surname: ABUBAKAR YAOUBA

Date and place of birth: November, 11th 1988 at Wum, Menchum Division North West Region Cameroon,

EDUCATION:

- **Bachelor:** 2008/2011**,**

  ADVANCED HIGHER TEACHERS TRAINING COLLEGE, ECOLE NORMALE SUPERIEURE (ENS) Bambili, University of Bamenda Cameroon DIPES 1, Mathematics / Physics.

- **Masters: 2017/2020,**

  ISTANBUL AYDIN UNIVERSITY Turkey, Electrical and Electronics Engineering

WORK EXPERIENCE:

- **2013/2017,** Mathematics teacher**, Government Bilingual High School Ngaoundere, Adamawa Region Cameroon**

- **2012/2013,** Physics/Mathematics teacher, **Government Bilingual High School Maroua, Extreme North Cameroon.**